NEW MODEL FOR THE 5-20 CM WAVELENGTH OPACITY OF AMMONIA PRESSURE-BROADENED BY METHANE UNDER JOVIAN CONDITIONS BASED ON LABORATORY MEASUREMENTS

A Master's Thesis

Presented to

The Faculty of the Division of Graduate Studies

By

Garrett Chinsomboon

Advisor Dr. Paul Steffes

In Partial Fulfillment

Of the Requirements for the Degree of

Master of Science in Electrical and Computer Engineering

Georgia Institute of Technology

December 2012

NEW MODEL FOR THE 5-20 CM WAVELENGTH OPACITY OF AMMONIA PRESSURE-BROADENED BY METHANE UNDER JOVIAN CONDITIONS BASED ON LABORATORY MEASUREMENTS

Approved by:

Professor Paul G. Steffes, Advisor
School of Electrical and Computer Engineering
Georgia Institute of Technology

Professor Gregory D. Durgin
School of Electrical and Computer Engineering
Georgia Institute of Technology

Professor Waymond R. Scott
School of Electrical and Computer Engineering
Georgia Institute of Technology

Date Approved: 12 November 2012

For the glory of the One who is

the First and the Last,

the Beginning and the End,

the Alpha and the Omega…

ACKNOWLEDGEMENTS

I would like to thank Dr. Paul G. Steffes for the marvelous opportunity to participate in this research. This is definitely an area of research I did not expect to find myself in, but this past year has definitely been both an eye-opening experience and a tremendous growth opportunity as I am able to explore a scientific field which is totally new to me. Thank you for your understanding during the challenges and encouragement during the successes. It was your kindness and wisdom that guided me through my graduate career. I would also like to extend my appreciation to the thesis panel members, Dr. Gregory Durgin and Dr. Waymond Scott, for providing me with your precious time to review this thesis and make valuable recommendations.

This work would not take place without the support of NASA Contract NNM06AA75C from the Marshall Space Flight Center supporting the Juno Mission Science Team, under Subcontract 699054X from the Southwest Research Institute. I thank the Juno mission team for the financial support; making it possible to complete this work.

My appreciation also goes out to my laboratory partners and the different people that helped me through this past year. Chris Barisich, thank you for always being available and willing to help in times of "lab crises". Pat Shahan, I am incredibly thankful for your positive attitude and helping hands. Danny Duong, Kiruthika Devaraj, and Bryant Karpowicz, thank you for your knowledge of the laboratory system and guidance throughout the year. I wish you all well in your future endeavors.

Moreover, thank you to all my family members. You have supported me from the very beginning and provided me with the will to complete my graduate studies. Mom – thank you for lessons of perseverance and for providing me with encouraging words when I needed to hear it most. Dad – thank you for your constant motivation and for being such a wonderful example for me; I long to become the man that you are. Most importantly, thanks be to God for His faithfulness and unfailing provisions. Praise be to Lord Jesus, without whom my life would be lost and my very existence without purpose.

but those who hope in the LORD
will renew their strength.
They will soar on wings like eagles;
they will run and not grow weary,
they will walk and not be faint.

Isaiah 40:31

CONTENTS

LIST OF TABLES

LIST OF FIGURES

SUMMARY

In order to fully understand the role methane (CH_4) plays in the microwave emission spectra of the deep atmospheres of the outer planets, over 280 laboratory measurements of the opacity of ammonia in a methane environment have been made in the 5-20 cm wavelength range. All opacity measurements were made with either 100 or 200 mbars of ammonia and with 1 to 3 bars of added methane in the 330-450K temperature range. A formalism for the absorptivity of ammonia broadened by methane has now been developed and had been applied to the Hanley et al. (Icarus, v. 202, 2009) model for the opacity of ammonia. Due to methane's relatively low abundance at Jupiter (~0.2% by volume), its effect on the microwave spectrum which will be observed by the Juno MWR (Microwave Radiometer) will be minimal. However, these experimental results will significantly improve the understanding of the microwave emission spectrum of Uranus and Neptune where methane plays a more dominant role.

CHAPTER 1

INTRODUCTION

Juno, the spacecraft entrusted with the daunting task of unlocking the secrets of Jupiter, is currently en route to the gas giant and is scheduled to arrive in 2016. In order to investigate this world beyond our own, countless technologies have been introduced so as to better understand the structure, composition, and evolution of Jupiter. Juno will provide us with an understanding of Jupiter with details at a scale never previously imagined. Among one of its mission objectives is to conduct a thorough analysis of the planet's atmosphere to determine the composition. The Juno microwave radiometer (MWR) will be instrumental in measuring the emission of Jupiter's atmosphere at the centimeter wavelengths. Since the microwave emission spectrum is determined by the microwave absorption of atmospheric constituents, understanding the microwave properties of such constituents is necessary so as to retrieve their abundances from the measured emission. As described in previous works by Hanley et al. (2009) and Karpowicz and Steffes (2011), ammonia and water vapor are known to be the principle microwave absorbing gases in the jovian atmosphere. Their opacity is related to their abundance, pressure, and temperature of the atmosphere, which is composed of mostly hydrogen and helium. However, it has been demonstrated by Devaraj (2011) that other (minor) constituents may also affect the absorption spectrum of ammonia by an effect known as pressure broadening. The laboratory measurements (described in this thesis) present the effects of methane (a minor constituent in the atmosphere of all gaseous planets) on the microwave absorption spectrum of ammonia. This information will enable us to better interpret the emission spectra we collect

when Juno arrives at Jupiter and develop a better understanding of the atmospheres of the other Jovian planets containing even larger amounts of methane.

1.1 Background

The jovian planets are the largest bodies in our solar system and they account for 99.56% of the planetary mass of the solar system. The largest of these planets, Jupiter, was first observed by Galileo Galilei in 1610 (see, e.g., Stillman, 1978). The constituents in the atmospheres of these jovian planets represent samples of the primordial cloud (from which our solar system is believed to have originated) in its truest form. By developing a better understanding of these constituents, we may be able to obtain vital information about our entire solar system.

Jupiter has been extensively studied with both ground-based and spacecraft-based observations in the microwave region. Out of the seven spacecraft that visited Jupiter, only the Galileo entry probe has entered into the atmosphere of Jupiter and taken measurements. Although the main constituents of Jupiter's atmosphere consist of hydrogen and helium, small traces of hydrogen sulfide, ammonia, methane, water vapor and other gases have also been detected. Only an approximate relative abundance of these gases is known on a planet-wide basis. The Juno MWR employs 6 separate radiometers (0.6, 1.25, 2.6, 5.2, 10 and 22 GHz) and is capable of probing Jupiter's atmosphere in the 1.3 cm – 50 cm wavelength region. Centimeter wavelengths are useful for probing the middle to deep atmospheres of the jovian planets, where the pressure ranges up to hundreds of bars.

1.2 Motivation

Various models for the formation of Jupiter exist that depend on the accurate knowledge of constituent abundances in Jupiter's atmosphere. It is difficult to validate the accuracy of these theories without an accurate knowledge of the atmospheric composition. Accurate microwave laboratory measurements are necessary to better simulate and model the microwave emission from the atmosphere of Jupiter in order to accurately retrieve the abundance of microwave-absorbing constituents. Therefore, laboratory measurements of these gases under simulated planetary atmospheric conditions are essential to further our understanding of the absorption spectra at Jupiter. Ultimately, better models for the microwave absorptivity can be developed based on the laboratory results obtained.

This work includes 288 microwave opacity measurements of either 100 or 200 mbar ammonia pressure-broadened by up to 3 bars of methane at temperatures ranging from 330K to 450K in the 5-20 cm wavelength region. A model for this methane-broadening effect has been developed by adjusting the methane-broadening free parameters to obtain the best data fit. This new model is an extension of the pure ammonia model described in Hanley et al. (2009). In order to verify that the measured effects were only due to the broadening by methane and not its intrinsic absorption, an additional experiment was conducted using 40 bars of methane pressure-broadened by hydrogen to a total pressure of 80 bars. This additional experiment confirmed the microwave transparency of methane. The planetary atmospheric simulator at Georgia Tech was utilized to collect data for both the ammonia-methane and the methane-hydrogen experiments.

From experimental data, it has been found that methane will indeed increase the microwave opacity of ammonia in the centimeter-wavelength region. Through comparisons with previous

ammonia-broadening models, it is found that the broadening parameter for methane is considerably larger than that of hydrogen and helium, as described by Hanley et al. (2009). Yet, the impact on ammonia opacity of helium and hydrogen is expected to be more significant than that of methane because these constituents are more abundant at Jupiter. Due to methane's relatively low abundance at Jupiter (~0.2% by volume), its effect on the microwave spectrum which will be observed by the Juno MWR will be minimal. However, these experimental results will significantly improve the understanding of the microwave emission spectrum of Uranus and Neptune, where methane has a more significant abundance (~2%-4%).

1.3 Organization

This thesis includes the discussion of basic electromagnetics concepts, the centimeter-wavelength measurement system, the measurement procedure, the data processing techniques, the corresponding uncertainties, the obtained laboratory measurements and the resulting model for microwave opacity. They are organized in the following manner:

Chapter 2.1 includes the required electromagnetic theory and the fundamental relationships necessary to calculate microwave absorption.

Chapter 2.2 illustrates the outdoor centimeter-wavelength measurement system at Georgia Tech. This section describes the planetary atmospheric simulator, the centimeter-wavelength subsystem and the data acquisition subsystem.

Chapter 2.3 outlines the steps taken to collect the necessary data and highlights the data processing procedure.

Chapter 2.4 discusses the uncertainty of measurements in detail. This section introduces the sources of the uncertainties, illustrates the calculations of the errors and discusses the impact they have on the final opacity model.

Chapter 3 presents the data taken with the measurement system and provides a model for the opacity of ammonia pressure-broadened by methane based on the collected data. This section also describes the optimization of the model by fitting it to the laboratory measurements.

Chapter 4 summarizes this work and includes a discussion about the impact of this model on the Juno mission and its applications for other planets in our solar system.

CHAPTER 2

EXPERIMENT DESIGN, THEORY, AND UNCERTAINTIES

Before a consistent model for the opacity of ammonia pressure-broadened by methane can be developed, it is essential to understand the underlying theory behind the data collection procedure. Data processing can only take place when there is a sufficient knowledge of the measurement theory. This section outlines the electromagnetics underlying the measurements and how they are used to compute the microwave opacities.

The expression of the electric and magnetic fields of an electromagnetic wave propagating in the $+x$ direction through an isotropic, homogeneous and lossy medium are given (in their phasor form) by:

$$\mathcal{E}(x) = \mathcal{E}_0 e^{-jkx} = \mathcal{E}_0 e^{-\alpha x} e^{-j\beta x} \tag{2.1}$$

$$H(x) = H_0 e^{-jkx} = H_0 e^{-\alpha x} e^{-j\beta x} \tag{2.2}$$

where $\mathcal{E}_0$ is the amplitude of the electric field, H_0 is the amplitude of the magnetic wave, k is the wave number, α is the attenuation constant and β is the phase constant. The wave number is calculated as

$$k = \omega\sqrt{\mu\varepsilon} \tag{2.3}$$

where ω is the angular frequency of the propagating wave, μ is the permeability of the medium and ε is the permittivity of the medium. In this work, the μ for all gases under jovian conditions is considered to be equal to the permeability of free space, μ_0. The permittivity for lossy gases is given by

$$\varepsilon = \varepsilon' - j\varepsilon'' \tag{2.4}$$

Substituting this into the equation for wave number gives

$$k = \omega\sqrt{\mu(\varepsilon' - j\varepsilon'')} \tag{2.5}$$

The wave number k can be rewritten in terms of the attenuation constant α and the phase constant β (Ramo et al., 1994)

$$jk = \alpha + j\beta = j\omega\sqrt{\mu\varepsilon'\left[1 - j\left(\frac{\varepsilon''}{\varepsilon'}\right)\right]} \tag{2.6}$$

where the attenuation constant is expressed as

$$\alpha = \omega\sqrt{\left(\frac{\mu\varepsilon'}{2}\right)\left[\sqrt{1 + \left(\frac{\varepsilon''}{\varepsilon'}\right)^2} - 1\right]} \tag{2.7}$$

and the phase constant is expressed as

$$\beta = \omega\sqrt{\left(\frac{\mu\varepsilon'}{2}\right)\left[\sqrt{1 + \left(\frac{\varepsilon''}{\varepsilon'}\right)^2} + 1\right]} \tag{2.8}$$

The ratio of α over β can be taken to remove the frequency dependence

$$\frac{\alpha}{\beta} = \sqrt{\frac{\sqrt{1+\left(\frac{\varepsilon''}{\varepsilon'}\right)^2} - 1}{\sqrt{1+\left(\frac{\varepsilon''}{\varepsilon'}\right)^2} + 1}} \tag{2.9}$$

with the ratio $\frac{\varepsilon''}{\varepsilon'}$ equal to $\tan\delta$ or the loss tangent of the medium. The quality factor of this medium is equivalent to the inverse value of the medium's loss tangent $\left(Q = \frac{\varepsilon'}{\varepsilon''}\right)$. For a low-loss gaseous medium

$$\frac{\varepsilon''}{\varepsilon'} = \tan\delta = \frac{1}{Q_{gas}} \ll 1 \tag{2.10}$$

with Q_{gas} being the quality factor of the gas. Therefore, the ratio of α over β of a low-loss gas can be approximated, with the Taylor series expansion, as

$$\frac{\alpha}{\beta} \approx \frac{\varepsilon''}{2\varepsilon'} \tag{2.11}$$

This method of approximation estimates $\frac{\alpha}{\beta}$ to within 0.5% of the actual ratio when the loss tangent is less than 0.01, which is almost always the case for a gaseous medium (Spilker, 1990).

2.1 Measurement Theory

The method utilized to determine the absorption of the gas in the resonator is determined through the lessening in the quality factor of the resonances in the presence of a lossy gas (Hanley and Steffes, 2007). The unitless quantity Q or the quality factor of a resonance is defined as (Matthaei et al., 1980)

$$Q = \frac{2\pi f_0 \times Energy\ Stored}{Average\ Power\ Loss} \tag{2.12}$$

with f_0 being the center frequency of the resonance. The quality factor, Q, is calculated by dividing this center frequency by the half-power bandwidth (HPBW)

$$Q = \frac{f_0}{HPBW} \tag{2.13}$$

The absorptivity, α, of the gas is related to its Q by

$$\alpha \approx \frac{\varepsilon''\pi}{\varepsilon'\lambda} = \frac{1}{Q_{gas}}\frac{\pi}{\lambda} \tag{2.14}$$

where ε' and ε'' represent the real and imaginary components of the gas' permittivity respectively, λ is the wavelength expressed in km and the resulting opacity α is in the units of Nepers/km (note that 1 Neper = 8.686 dB). The quality factor of a resonator loaded with a lossy test gas is given by

$$\frac{1}{Q_{loaded}^{m}} = \frac{1}{Q_{gas}} + \frac{1}{Q_r} + \frac{1}{Q_{ext1}} + \frac{1}{Q_{ext2}} \tag{2.15}$$

with Q_{loaded}^{m} being the measured quality factor of the loaded resonator, Q_{gas} being the quality factor of the gaseous medium under investigation, Q_r being the quality factor of the evacuated cavity resonator without coupling losses and both Q_{ext1} and Q_{ext2} being the external coupling losses of the resonator's coupling probes. According to Hanley and Steffes (2007), Q_{ext1} is equivalent to Q_{ext2} since a symmetrical resonator is used to collect laboratory measurements in this work. The transmissivity can be used to calculate the coupling losses Q_{ext} and is given by

$$t = 10^{-S/10} \tag{2.16}$$

where S is the insertion loss (in dB) of the resonator at the frequency of a given resonance (Matthaei et al., 1980). The relationship between the value for transmissivity and the coupling losses is described as

$$t = \left[\frac{2\,Q^{m}}{Q_{ext}}\right]^{2} \tag{2.17}$$

and solving for the coupling losses gives

$$Q_{ext} = \frac{2Q^{m}}{\sqrt{t}} \tag{2.18}$$

where Q^m is the measured quality factor. The measured quality factor of the resonator at vacuum Q_{vac}^m is related to Q_r by

$$\frac{1}{Q_{vac}^m} = \frac{1}{Q_r} + \frac{1}{Q_{ext1}} + \frac{1}{Q_{ext2}} \tag{2.19}$$

Substituting the relationship for Q_{ext} into the equation for Q_{vac}^m and Q_{loaded}^m gives

$$\frac{1}{Q_{gas}} = \frac{1-\sqrt{t_{loaded}}}{Q_{loaded}^m} - \frac{1-\sqrt{t_{vac}}}{Q_{vac}^m} \tag{2.20}$$

where t_{loaded} and t_{vac} represent the transmissivity at loaded and vacuum conditions respectively. The magnitude of the shift in the peak frequencies of the resonances depends on the refractive index of the gas present. The quality factor also changes along with the center frequency due to the variations in the coupling losses; this effect is known as dielectric loading (DeBoer and Steffes, 1994). The dielectric loading effect can be mitigated by shifting the desired resonance of a lossless gas by the same amount as that of the test gas and taking additional measurements of the quality factor and transmissivity under those conditions. These dielectric matching measurements replace Q_{vac}^m and t_{vac} to give the final equation for calculating the opacity. The relationship for absorptivity is converted from the units of Nepers/km into dB/km (1 Neper/km = 8.686 dB/km) and is given by

$$\alpha = 8.686\ \frac{\pi}{\lambda}\left(\frac{1-\sqrt{t_{loaded}}}{Q_{loaded}^m} - \frac{1-\sqrt{t_{matched}}}{Q_{matched}^m}\right) \qquad (dB/km) \tag{2.21}$$

It is also important to know the refractive index n_{ri} of the gas under test since small changes in this value could alter the way the electromagnetic waves propagate through the medium. Although n_{ri} is known to be very close to unity for most gases, the frequency shift exhibited by

the resonances can be used to determine this refractive index to a high level of accuracy. The refractivity (N) is given by

$$N = 10^6(n_{ri} - 1) \tag{2.22}$$

The refractivity is measured by comparing the center frequency of the resonances under gaseous conditions to the peak frequency of the resonances at vacuum and is given by

$$N = \frac{10^6(f_{vac} - f_{gas})}{f_{gas}} \tag{2.23}$$

where N is the refractivity of the entire gas mixture, f_{gas} is the peak frequency of the resonance in the presence of the test gas and f_{vac} is the peak frequency of the resonator at vacuum (Tyler and Howard, 1969). The overall refractivity of the mixture is the sum of the refractivity of the individual gases scaled with their respective mole fractions. In order to remove the temperature and pressure dependencies of the refractivity value, the normalized refractivity can be computed as follows

$$N' = \frac{NRT}{P} \qquad (cm^3 \cdot molecule^{-1}) \tag{2.24}$$

where T is the temperature in K, P is the pressure of the test gas in bars and R is the gas constant equal to 1.38065×10^{22} bar·cm^3·molecule^{-1}·K^{-1}.

The asymmetry calculation is helpful in determining whether a particular resonance is corrupted by an overlapping resonance of lower Qs as well as in quantifying the associated measurement uncertainties. According to DeBoer and Steffes (1996), the asymmetry (A) is given as

$$A = 100\,\frac{(f_h - f_c) - (f_c - f_l)}{(f_h - f_l)}\,\% \tag{2.25}$$

where f_h is the upper -3 dB frequency, f_l is the lower -3 dB frequency and f_c is the center frequency of the resonance. Only the resonances with low asymmetry (typically less than 5%) are used in order to prevent overlapping resonances broadening disproportionally and yielding inaccurate results (Hanley and Steffes, 2007).

2.2 High-Pressure Centimeter-Wavelength System

The Ultra-High Pressure System is utilized to collect microwave opacity measurements of pure ammonia and the ammonia-methane mixture in the 5-20 cm wavelength region. In this work, the system supported absorptivity measurements at temperatures up to 450 K and up to 3 bars in total pressure. The high-pressure measurement system is composed of the planetary atmospheric simulator, centimeter-wavelength subsystem and the data handling subsystem. The current configuration of the outdoor measurement system at Georgia Tech is illustrated in Figure 1 and Figure 2.

2.2.1 The Planetary Atmospheric Simulator

The planetary atmospheric simulator is responsible for controlling the conditions and environment of the cylindrical cavity resonator, including the pressure and the temperature of the test gas. The simulator was designed by Karpowicz and Steffes (2011); it consists of a high-pressure vessel, temperature chamber, mass flow meter, vacuum pump, gas valves, pipelines, high-pressure gas bottles, pressure gauges and temperature gauges.

The main component of the simulator is the pressure vessel, which contains the microwave resonator, capable of handling pressures up to 100 bars and temperatures up to 520 K. The cylindrical vessel was custom built by Hays Fabrication and Welding (Springfield, OH) and has

an internal volume of 32.3 L and weighs approximately 544.3 kg. The stainless-steel vessel was sealed with a composite glass fiber/nitrile butadiene rubber KLINGERsil® C-4430 O-ring and 20 nuts, which were 6 cm (2-3/8 in.) in diameter and torqued to 1762 N-m (1300 lb-ft) of torque. The pressure vessel has two 1.27 cm (0.5 in.) NPT input ports (one for gas inlet and one for the temperature sensor), two CF-1.33 flanges of 3.38 cm (1.33 in.) in diameter for microwave feedthroughs and a 6.35 mm (0.25 in.) NPT port for the gas outlet. Hays Fabrication and Welding tested the pressure vessel to ensure the integrity of all flanges and feedthroughs at the pressure of 100 bars before delivery. The pressure vessel has an outside diameter of 35.56 cm (14 in.) and is constructed out of a 30.48 cm section of the schedule 100 pipe. The maximum interior height of 46.04 cm (18-1/8 in.) was achieved by welding the elliptical head to the bottom of the pressure vessel. The 9.2 cm (3-5/8 in.) thick top plate accompanies the top of the pressure vessel which is a 10.16 cm (4 in.) thick ANSI class 900 flange.

Since the combined weight of the pressure vessel and the Grieve® industrial oven model AB-650 temperature chamber (rated to the temperature of 615 K and weighs 739 kg) exceeded the allowable limit of the laboratory floor, an outdoor concrete pad was instead used for this load. For this reason, all system components, except the data acquisition subsystem and the microwave network analyzer, were placed outside where a decommissioned crane was once situated. The outdoor system, including the pressure vessel contained in the temperature chamber, is shielded from weather conditions by a metallic EZEE® shed.

A GE Druck DPI 10430A Digital Test Gauge was used to make pressure measurements in the 0 to 2 bar range while the GE Druck DPI 104300A Digital Test Gauge was used in the 2 to 20 bar range. While the GE Druck 10430A Digital Test Gauge has a resolution of 0.1 mbar, the GE Druck DPI 104300A Digital Gauge has a resolution of 1 mbar. The gauges display the absolute

pressure within the pressure vessel and have 0.05% full scale error band accuracy. Both are powered by a 9 V external power source and communicate via RS-232 serial interfaces. At pressures of above 20 bars, the pressure transducer is employed to make the pressure measurements within the pressure vessel. The Omega® pressure transducer measures absolute pressure and has an accuracy of ±0.25% full scale output. It is attached to the T-connector in the pipe leading to the gas inlet that goes within the pressure vessel. The HP multimeter model 34401A, which is situated indoors, is responsible for measuring the voltage output of the pressure transducer.

The Omega® resistance temperature detector (RTD) model PRCU-10-2-100-1/4-9-E is utilized to monitor the gases' temperature within the pressure vessel. The resolution of the RTD is 0.01°C and the device has an accuracy of ±0.15°C at 0°C and ±0.55°C at 200°C (IEC/DIN Class A). Through a 1/4" Swagelok® tube to 1/2" NPT adapter (SS-400-1-8BT), the RTD is connected to 1/2" NPT port of the pressure vessel.

Gas bottles used for opacity measurements (ammonia and methane) and dielectric matching (argon) are arranged outside the EZEE® shed in a six-pack cylinder rack. All gas bottles were provided by Airgas Inc. and were of Ultra-High Purity UHP300 grade. The gases are fed from the bottles into the pressure vessel through a series of valves, tubing and regulators. The Airgas® model Y11E444B660, Matheson® model 3030-350 and Matheson® model 3030-580 were used as the gas delivery regulator for ammonia, methane and argon respectively. The 3/8" outer diameter stainless steel and Swagelok® fittings connect the gas handling subsystem and delivers the gas into the pressure vessel. When the pressure vessel is to be evacuated, the system is vented down to near ambient pressure before a vacuum is taken with the Welch DuoSeal® vacuum pump model 1376B-01.

The mass flow meter, Teledyne-Hastings HFM-I-401 industrial flow meter, is tested to withstand 103 bars of pressure and is used to monitor the gas flow into the pressure vessel. The estimation of the total gas volume within the pressure vessel is achieved by utilizing the flow *totalizer* function of the mass flow meter as gas is being added because volume changes along with temperature by a measureable amount. Figure 1 displays the outdoor system components along with the gas cylinder rack and the metallic EZEE® shed. The valves shown in black are Swagelok® model SS-1RS6 valves (rated to 93°C at 195 bars) and valves shown in blue are Swagelok® model SS-1RS6-PK valves (rated to 315°C at 215 bars).

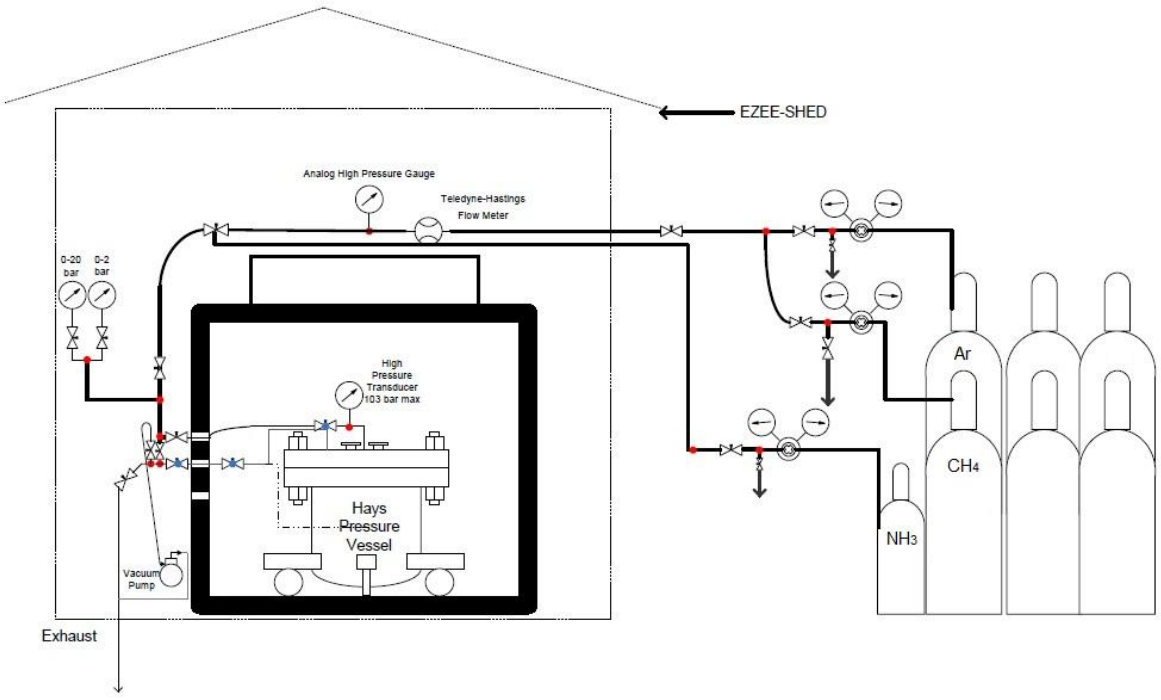

Figure 1: The Georgia Tech high-pressure system used for collecting centimeter-wavelength microwave opacity measurements (Karpowicz and Steffes, 2011). High-temperature valves are shown with a blue dot

2.2.2 Centimeter-Wavelength Subsystem

The pressure and temperature ratings of the components used were a major consideration when the microwave measurement system and data acquisition system were designed. Over the past twenty-eight years, the microwave subsystem has undergone continuous renovations; improving speed, accuracy and reliability of the microwave instruments (see, e.g., DeBoer and Steffes, 1996; Hanley and Steffes, 2007).

A 304 stainless steel cylindrical cavity resonator is contained within the pressure vessel. It has an inner radius of 13.12 cm with an inner height of 25.75 cm and is optimized for measurements in the 5-20 cm wavelength region. The interior surface of the resonator is plated with gold in order to prevent corrosion due to reactive gases and improve the quality factor of the resonances. The two closed-loop probes, mounted on the top of the resonator, are oriented to optimize the quality factor of the $TE_{(0,M,L)}$ modes. The two horizontal slits on the side of the resonator are located near the top plate in order to suppress the undesired TM resonant mode and allow gas entry into the resonator interior. Both the top and bottom plates of the resonator are separated approximately 1.75 mm from the cylindrical body with Teflon® washers around the connecting screws in order to eliminate the degenerate $TM_{(1,M,L)}$ resonant modes. Although this separation increases the sensitivity of the system, more microwave energy is allowed to leave the resonator. A stainless steel mesh screen is wrapped around the resonator to dampen the escaped microwave energy reentering the resonator after reflecting off the inner walls of the pressure vessel. The quality factors of the resonances of the cylindrical cavity resonator range from 30,000 to 80,000. The two ports on the top plate of the resonators are essentially symmetrical.

The Transverse Electric (TE) and Transverse Magnetic (TM) mode frequencies of the cylindrical cavity resonator are calculated as

$$f_{TE(N,M,L)} = \frac{c}{2\pi\sqrt{\mu_r \varepsilon_r}} \sqrt{\left(\frac{p_{n,m}}{r}\right)^2 + \left(\frac{\pi L}{h}\right)^2} \tag{2.26}$$

$$f_{TM(N,M,L)} = \frac{c}{2\pi\sqrt{\mu_r \varepsilon_r}} \sqrt{\left(\frac{q_{n,m}}{r}\right)^2 + \left(\frac{\pi L}{h}\right)^2} \tag{2.27}$$

with c representing the speed of light in cm/s, μ_r is the real part of the relative permeability inside the resonator, ε_r is the real part of the relative permittivity inside the resonator, r is the internal radius of the resonator in cm, h is the height of resonator in cm, $q_{n,m}$ is the M^{th} zero of the N^{th} order Bessel function of the first kind and $p_{n,m}$ is the M^{th} zero of the first derivative of the N^{th} order Bessel function of the first kind (Pozar, 1998). The subscripts N, M and L denote the number of zeros in the standing wave patterns in the circumferential, radial and axial dimensions respectively. Only TE modes are measured in the laboratory experiments due to their higher quality factors. On the contrary, the TM modes have been intentionally suppressed to reduce the level of interference with the favorable TE modes (Hanley, 2008). A dozen high Qs with low asymmetry are used as "standard resonances", Hanley et al. (2009) describes the selection criteria for these resonances in great detail.

High-pressure Ceramtec® feedthroughs are connected to the resonator within the pressure vessel through Times Microwave® SiO_2 microwave cables. These cables are responsible for coupling the energy into and out of the pressure vessel and are capable of withstanding temperatures of up to 875 K. The two SMA Ceramtec® feedthroughs (model 16545-01-CF) on the exterior of the pressure vessel are rated to 103 bars and 625 K; they are both backed by annealed copper gaskets (Karpowicz and Steffes, 2011). Type-BNC connectors are fitted to two 1 m long sections of

high-temperature RG-214 cable, and were connected to the Ceramtec® feedthroughs through high-temperature type-BNC to SMA connectors. The cables were assembled with high-temperature solder rated at 650 K. The two 24.4 m Andrews® CNT 600 microwave cables (rated to 350 K) connect the RG-214 cables emerging from the oven to an Agilent® E5071C vector network analyzer within the laboratory. The length of the Andrews® CNT 600 microwave cables ensures that the network analyzer could be placed within laboratory environments to prevent it from experiencing temperature fluctuations. The data acquisition laptop computer then obtains the measured S-parameters from the network analyzer via GPIB.

2.2.3 Data Acquisition Subsystem

The data acquisition subsystem consists of a laptop computer and a data logging computer. The laptop computer is connected to the network analyzer and multimeter through a GPIB connected to National Instruments® NI-488.2 interface card. The data logging computer interfaces with the pressure and temperature sensors through USB to RS-232 adapters and extended USB buses. These extended connections allow the data logging computer to be located indoors even though the sensors are a part of the outdoor system. The network analyzer located within the laboratory operates from 300 kHz to 8.5 GHz; Option 1E5 provides it with high-stability timebase. Both the temperature and pressure sensors are controlled and monitored through Python® code. The network analyzer is controlled via Matlab® through SCPI (Standard Commands for Programmable Instruments). The Matlab® software utilized for data acquisition in this work is similar to that described in Hanley and Steffes (2007); a more elaborate description of the entire data acquisition subsystem is provided by Karpowicz (2010). Figure 2 displays the block diagram of the interface between the outdoor centimeter-wavelength system and the data acquisition subsystem within the laboratory.

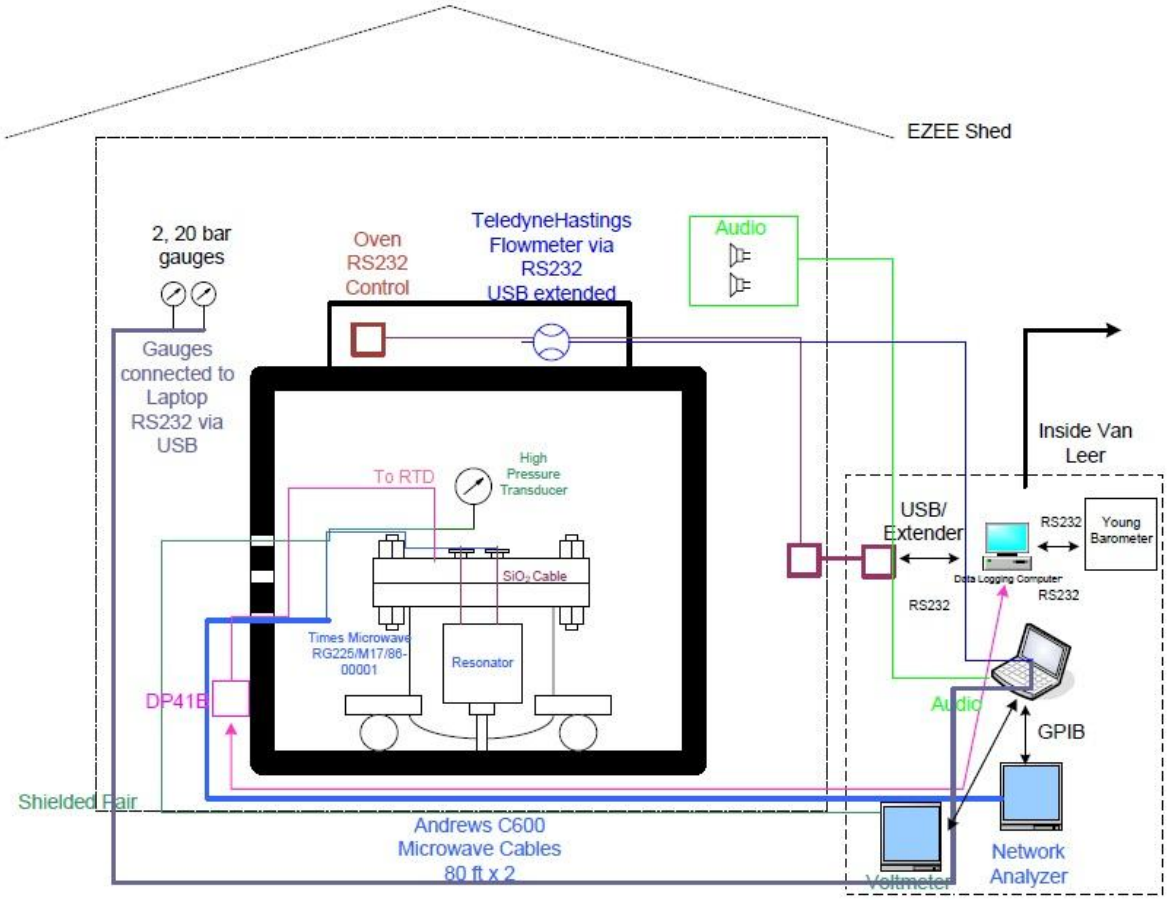

Figure 2: The block diagram of the centimeter-wavelength outdoor system and the data acquisition subsystem (Karpowicz and Steffes, 2011).

2.3 Measurement Procedure

In order to begin taking measurements, it is essential to make sure the outdoor gas containment system has no leaks. This not only guarantees that the toxic or flammable gas does not escape to the surrounding atmosphere, but also reduces uncertainties associated with constituent partial pressures. A leak-detection liquid is utilized during positive-pressure tests so as to verify the integrity of the pipes, pressure vessel, valves and regulators and ensure that the gas handling system is leak-proof at high pressures. The pressure vessel is sealed at low temperatures so that

the seal will improve as the sealant material expands at higher temperatures and ensures that the pressure vessel remains leak-proof. When a vacuum is drawn in the pressure vessel, the additional compression force due to atmospheric pressure fortifies the tightening by pressing in on the external surface of the pressure vessel. High-pressured argon (at 95 bars) is discharged into the pipes and the pressure is monitored with the pressure gauge on the regulator until it is determined that a good seal has been established. Since the gas handling system is outdoors, it is vulnerable to ambient temperature swings. Small temperature changes will also result in a variation in pressure, therefore, several days must be spent monitoring the pressure to ensure that no gas has in fact escaped.

It is easier to make changes to the mixing ratio and pressure of gases in the pressure vessel than to change the temperature of the system. As a result, sets of measurements are taken at a particular temperature with multiple pressures, concentrations and mixing ratios before measurements at a different temperature are taken. Once all measurements are completed at one temperature, the set point for the industrial oven is adjusted to bring the temperature chamber to a new temperature for the subsequent experiments.

Physisorption occurs when gaseous molecules of a substance (the adsorbate) adhere to the surface of a solid or liquid material (the substrate) due to weak van der Waals attraction between the two (Devaraj, 2011). When the gases are added to the system, the gaseous molecules are likely to physically adsorb to the walls of the pressure vessel. According to Young and Crowell (1962), the formation of the physically adsorbed layer is similar to the condensation of a vapor to form a liquid when the gas nears its condensation point but this can also occur under lower pressure and warmer conditions. All gaseous molecules are prone to this effect. However, polar molecules are more likely to undergo physisorption especially in conductive substrates. The

adsorbed molecules do not behave in the same manner as the ones in gaseous form in the presence of an electromagnetic wave and will also change the electrical conductivity of the surface responsible for the adsorption (Young and Crowell, 1962). The changes in conductivity and quality factors of the resonator due to the adsorption of ammonia, however, is determined to be minimal and negligible (Devaraj, 2011). There are two primary methods to return the adsorbed molecules to its gaseous form (desorption). The first method is to reduce the partial pressure of the adsorbate while the second is to raise the temperature of the substrate, providing enough energy to break the weak van der Waals forces that are holding the adsorped gas in place.

Rodrigues and Moraes (2002) concluded that the physisorption of ammonia increases with higher concentration across all temperatures and decreases with an increase in temperature for all concentrations. Also, they reported that temperature plays a more significant role in adsorption than concentration. Although ammonia is the gaseous compound being studied, other polar molecules behave in a similar manner. Even though the effects of adsorption are understood, it is still difficult to predict because of the dependence on the substrate's molecular structure. Since adsorption can seriously alter the concentration of the test gas in the pressure chamber, precautions must be taken to account for this effect.

A method to compensate for the adsorption effect is to saturate the surface of the gas handling system with a layer of ammonia before the measurements are taken. Since only a limited number of adsorbate layers can form, any additional gas added would not adsorb after the substrate surface is fully saturated. This process includes first adding ammonia to the system and letting it saturate the surface of the gas handling system while monitoring the quality factors inside the resonator. As ammonia is introduced into the system, a reduction of the quality factors of each resonance is expected as ammonia absorbs microwave energy. Afterwards, as ammonia begins to

adsorb to the internal walls of the gas handling system, the quality factors will increase slightly. Once the quality factors stabilize, the internal surface is said to be fully saturated, at this point, the rate of adsorption and desorption is equal. Only after the ammonia abundance is stable are measurements taken, and then the pressure-broadening methane is added to the system.

The first set of measurements of the predetermined resonances is taken under vacuum conditions at the desired temperature. The next step is to add the test gas (ammonia) to the system once it is thermally stabilized. Due to the outdoor system's large volume and huge thermal time constant, the time needed for stabilization with the test gas is 8 to 10 hours. Once the system is stabilized and the necessary measurements are taken, methane is added as the broadening gas. The frequency shifted resonances are then again measured. After measurements are conducted using several different pressures of methane, a second vacuum is drawn. After venting down to atmospheric pressure, the vacuum pump is run for at least 12 hours to ensure that the remaining test gases have been evacuated. A second set of vacuum measurements are taken at the desired temperature. The dielectric matching process consists of shifting the resonances by the same amount as that of the test gas mixture using a highly refractive and microwave transparent gas (argon). The experimenter is aided by a series of tones produced by the data acquisition computer to indicate whether a peak frequency match is made. Measurements of the quality factors of each resonance are recorded as dielectric matches are made with the reference gas. Finally, a third and final vacuum is drawn in the system so as to evacuate the matching gas, and the necessary measurements of center frequency and quality factor of each resonance are taken. Following this step, three sets of straight-through measurements of the signal levels are made. This is achieved by detaching the RG-214 cables from the Ceramtec® feedthroughs and connecting them directly to each other (without the presence of the resonator) through a high-

temperature female-to-female BNC connector. The three sets of transmissivity measurements are taken at the standard resonance frequencies. The purpose of taking straight-through measurements is to quantify the losses in the cables and to correct for transmissivities in both the loaded and matched measurements. The coax connections are disconnected and reconnected between each set of transmissivity measurement in order to better statistically characterize the reproducibility of the electrical connections (Devaraj, 2011). The process of collecting transmissivity measurements includes opening the industrial oven door to disconnect and reconnect the cables and may result in a temporary temperature variation. All transmissivity measurements are taken at the end of the experiment set to ensure that the resonator remains at a constant temperature, within the ±0.1°C margin. Usually a week and a half is needed to complete the entire process, from the first vacuum measurement to the final transmissivity measurement.

2.3.1 Data Processing

The experimental data is processed after each complete experiment sequence is completed. The Matlab® software used to process the data is similar to that described in Hanley and Steffes (2007) with minor alterations to represent the recent modifications made to the system. This software is responsible for loading the raw data, running the smoothing algorithm, and calculating the microwave opacity of the test gas at a given frequency, temperature, concentration, mixing ratio and pressure.

Variations in the transmissivity of the cables are deconvolved from the measured sweeps. At each pressure, an average value for the cable transmissivity is calculated for each resonance. This is obtained by taking the mean value of the average of the set of sweeps from the three measurements. The insertion loss of the loaded condition (S_l) is calculated by subtracting this

average value from the peak power measurements of each resonance with the test gas present. Similar steps are used to calculate the insertion loss of the matching condition (S_m). Second vacuum measurements are utilized in data processing most since they are taken temporally closest to both the measurements of the test gas and the matching gas. The first and third vacuum measurements are also compared to the second measurement to ensure that there is consistency throughout the entire experiment set. These insertion loss values are used in the calculation of t_{loaded} and $t_{matched}$, as illustrated in Equation 2.16.

2.4 Measurements Uncertainties

Uncertainties associated with centimeter-wavelength opacity measurements are due to 5 different types of errors. These uncertainties arise due to instrumental errors (Err_{inst}), errors in dielectric matching (Err_{diel}), errors in transmissivity (Err_{trans}), errors due to asymmetry in resonances (Err_{asym}) and errors due to uncertainties in the measured environmental conditions (Err_{cond}). Instrumentation errors arise because of the microwave test equipment's limitations. Both the sensitivity of the electrical system and the ability of the system to accurately measure bandwidths ($BW_{measured}$) and peak frequencies (f_0) make up the instrumental errors of the opacity measurements. Errors in dielectric matching arise from small mismatches in the alignment of the center frequencies of the test and matching gas. Transmissivity errors are caused by uncorrected losses in the electronics, cables, adapters and waveguides in the system. This ultimately translates into an uncertainty in the power amplitude of the measurement of each resonance. The asymmetry errors are a result of the asymmetric nature of the resonances due to the overlapping of nearby undesired resonances. Lastly, the errors due to experimental conditions arise from uncertainties in the measured pressure, temperature and concentration. Err_{cond} does not alter the

processing of the opacity measurements themselves but plays a crucial role in the development of an accurate microwave opacity model. Of the various sources of errors introduced here, errors in dielectric matching are the least statistically significant due to the high accuracy of the data collection software while taking the loaded and matched measurements.

Noise of electronic components and the accuracies of the frequency references make up the overall electrical noise. This noise is calculated by taking the average of the instrumental uncertainty across multiple measurements. This is done as outlined in Hoffman et al. (2001), however, with an addition of the frequency sensitivity of the network analyzer. For instrumental errors, the best error estimate is given by the below relationship

$$Err_n = B \times \frac{S_n}{\sqrt{n_{samples}}} \tag{2.28}$$

where S_n is the sample standard deviation, B is the confidence coefficient and $n_{samples}$ is the number of independent measurements taken of the sample. The data collection system is configured to collect 30 sets of independent measurements for each resonance. The confidence coefficient B depends on the confidence interval used. In this work, a 95% confidence interval (approximately 2σ) is employed. The confidence coefficient is equivalent to the critical value of a Student t-test with a two-tailed significance of 0.05 and ($n_{samples} - 1$) degrees of freedom (Student, 1908). A 95% confidence interval means that the actual average will be both above and below the interval 2.5% of the time. For 30 samples, the confidence coefficient is 2.045. S_n consists of only the standard deviation of the resonances' bandwidth because the standard deviation of the center frequencies is extremely small and its effects on the quality factors is negligible.

When calculating Err_{inst}, the error in measuring the center frequency of resonance (Err_o) and the error in measuring the bandwidth of resonance Err_{BW} are taken into account. The Agilent E5071C-ENA Vector Network Analyzer used in this work was also utilized by Hanley et al. (2009), therefore Err_o is calculated in a similar fashion. The relative uncertainty in the frequency measurement is given as

$$Err_o = f_{measured} \times (5 \times 10^{-8} + 5 \times 10^{-7} \times years\ since\ calibrated) \quad \text{(Hz)} \tag{2.29}$$

where $f_{measured}$ is the measured frequency in Hz. According to Hanley et al. (2009), the absolute uncertainty can be as low as 1 ppm of the actual frequency measurement, thus this is deemed statistically insignificant. Since Agilent® did not provide specifications for calculating the error in the measured bandwidth, the formula given by Hanley et al. (2009) was used

$$Err_{BW} = \sqrt{2} \times BW_{measured} \times (5 \times 10^{-8} + 5 \times 10^{-7} \times years\ since\ calibrated) \quad \text{(Hz)} \tag{2.30}$$

where $BW_{measured}$ is the measured bandwidth in Hz. Both Err_o and Err_{BW} are 3σ uncertainties and must be multiplied by a factor of 2/3 to obtain 2σ uncertainties. These calculations represent the worst case scenario for instrumental uncertainties.

According to DeBoer and Steffes (1994), the computation for the worst case instrumental error is given by

$$Err_\psi{}^2 = \langle F_l{}^2 \rangle + \langle F_m{}^2 \rangle - 2\langle F_l\, F_m \rangle \tag{2.31}$$

where

$$\langle {F_i}^2 \rangle = \frac{\Upsilon_i^2}{f_{oi}^2} \times \left(\frac{Err_o}{Q_i^2} + Err_{BW}^2 + Err_{Ni}^2 + \frac{2Err_o Err_{BW}}{Q_i} \right) \quad i = l, m \tag{2.32}$$

$$\langle F_l \, F_m \rangle = - \frac{\Upsilon_l \, \Upsilon_m}{f_{ol} \, f_{om}} \times \left(\frac{Err_o^2}{Q_l \, Q_m} + Err_{BW}^2 + \frac{Err_o Err_{BW}}{Q_l} + \frac{Err_o Err_{BW}}{Q_m} \right) \tag{2.33}$$

$$Q_i = \left(\frac{f_{oi}}{f_{BWi}} \right) \quad i = l, m \tag{2.34}$$

$$\Upsilon_i = (1 - \sqrt{t}) \quad i = l, m \tag{2.35}$$

where the subscripts l and m represents the loaded and matched conditions respectively. Whereas f_{ol} and f_{om} are the measured center frequencies of each resonance for the loaded and matched case, Q_l and Q_m are the measured quality factors of each resonance for the loaded and matched case respectively . The 2σ instrumental uncertainties of the opacity measurements is given by

$$Err_{inst} = \frac{8.686 \, \pi}{\lambda} \, Err_{\psi} \text{ (dB/km)} \tag{2.36}$$

where λ is the wavelength given in km.

Uncertainties in dielectric matching, transmissivity and asymmetry are computed in the same fashion as Hanley et al. (2009) although some minor modifications were made to reflect recent changes in the data collection system. Dielectric mismatches and small misalignments of the center frequencies between the loaded and matched conditions give rise to errors in dielectric matching (Err_{diel}). Although the matching gas (argon) is lossless, the measured quality factor can still vary slightly from those measured at vacuum. Through the comparison of the Qs of the three vacuum measurements, this effect can be taken into account

$$\left(\frac{dQ}{df}\right)_i = \left|\frac{Q_{vac,i} - Q_{matched}}{f_{vac,i} - f_{matched}}\right| \quad i = 1, 2 \; and \; 3 \tag{2.37}$$

The dQ is then calculated using the maximum of the three values

$$dQ = \left(\frac{dQ}{df}\right)_{max} |f_{loaded} - f_{matched}| \tag{2.38}$$

with f_{loaded} being the frequency of the resonance when under loaded conditions and $f_{matched}$ being the frequency of the resonance when under matching conditions. The uncertainties of microwave opacity measurements due to dielectric mismatches can then be calculated as

$$Err_{diel} = \frac{8.686\,\pi}{\lambda} \times \left|\left(\frac{1-\sqrt{t_{loaded}}}{Q^m_{loaded}} - \frac{1-\sqrt{t_{matched}}}{Q^m_{matched}+dQ}\right) - \left(\frac{1-\sqrt{t_{loaded}}}{Q^m_{loaded}} - \frac{1-\sqrt{t_{matched}}}{Q^m_{matched}-dQ}\right)\right| \quad \text{(dB/km)} \tag{2.39}$$

Usually, the greatest contributor to the overall uncertainty of opacity measurements is uncertainty in transmissivity. It is caused by losses in the microwave instruments and other equipment (including the Vector Network Analyzer, cables, adapters and waveguides). This error is shown in the uncertainty of the measurement amplitude. The greatest error is caused by disconnecting and reconnecting the cables during transmissivity measurements. The RG-214 cables connected to the pressure vessel feedthroughs are disconnected and connected together in a thru-configuration through a high-temperature female-to-female BNC connector. The signal level measurements are taken thrice to generate three measurement samples. The cables are disconnected and reconnected together again between each set of measurement. The error in the measured signal level is given by

$$Err_{msl} = \frac{4.303}{\sqrt{3}}\, S_n \tag{2.40}$$

where S_n is the standard deviation of the sample cable loss measurements expressed in dB. The confidence coefficient of 4.303 is equal to the critical value of the 3-sample Student t-test at the 95% confidence interval (Student, 1908). Err_{msl} only takes into account the performance variations of the cables outside the pressure vessel which can be disconnected and reconnected but not the portion of the SiO_2 cable that lies within the pressure vessel. Therefore, an additional 0.25 dB is added to account for the worst-case variations in cable performance (Karpowicz and Steffes, 2011). Moreover, an additional 0.5 dB is also included in order to reflect variations in cable losses due to temperature fluctuations in the 15 m long outdoor section of the two 24.4 m long Andrews® CNT 600 microwave cables. The resulting uncertainty in the insertion loss of the system is given as

$$Err_{ins\ loss} = \sqrt{Err_{msl} + 0.25^2 + 0.5^2} \quad \text{(dB)} \tag{2.41}$$

The insertion loss is related to transmissivity error through the following relationship

$$Err_{t,i} = \frac{1}{2}\left(10^{-(S_i - Err_{ins\ loss})} - 10^{-(S_i + Err_{ins\ loss})}\right) \quad i = l, m \tag{2.42}$$

where the subscripts l and m represents the loaded and matched conditions respectively. S represents the resonator's insertion loss. The 2σ uncertainties in microwave opacity due to transmissivity is given by

$$Err_{trans} = \frac{8.686\,\pi}{2\lambda}\left(\frac{\sqrt{t_l + Err_{t,l}} - \sqrt{t_l - Err_{t,l}}}{Q^m_{loaded}} - \frac{\sqrt{t_m - Err_{t,m}} - \sqrt{t_m + Err_{t,m}}}{Q^m_{matched}}\right) \quad \text{(dB)} \tag{2.43}$$

The asymmetric nature of the measured resonances also contributes to the overall uncertainty of microwave opacity. The asymmetry is a result of off-axis/TM mode resonances overlapping the

axial/TE mode resonances. This uncertainty arises when loaded measurements experience disproportionate asymmetric broadening as compared to the matched measurements. This effect is more noticeable at lower temperatures and shorter wavelengths. The calculation of the bandwidth based on the higher and lower halves of each resonance will account for the asymmetric nature of the resonances

$$BW_{high} = 2 \times (f_{high} - f_{center}) \tag{2.44}$$

$$BW_{low} = 2 \times (f_{center} - f_{low}) \tag{2.45}$$

where BW_{high} and BW_{low} are full bandwidths based on the high and low sides of the resonance, f_{high} is the upper half-power frequency, f_{center} is the center frequency of the resonance and f_{low} is the lower half-power frequency. In order to characterize the error, the resulting opacities are calculated with BW_{high} and BW_{low} values. The difference in microwave opacity between the two calculations is regarded as the 2σ errors for Err_{asym}. The uncertainty due to resonance asymmetry is expressed as

$$Err_{asym} = \frac{8.686\,\pi}{\lambda} \times \left| \left(\frac{1-\sqrt{t_{loaded}}}{Q^m_{loaded,high}} - \frac{1-\sqrt{t_{matched}}}{Q^m_{matched,high}} \right) - \left(\frac{1-\sqrt{t_{loaded}}}{Q^m_{loaded,low}} - \frac{1-\sqrt{t_{matched}}}{Q^m_{matched,low}} \right) \right| \quad \text{(dB/km)} \tag{2.46}$$

where $Q^m_{loaded,high}$ and $Q^m_{loaded,low}$ are the computed quality factors for the loaded condition calculated with the high and low halves of the resonance, respectively. $Q^m_{matched,high}$ and $Q^m_{matched,low}$ are the computed quality factors for the matched condition calculated with the high and low halves of the resonance, respectively.

Uncertainty due to experimental conditions (Err_{cond}) takes into account the variations in temperature, pressure and concentration of the gaseous medium. Although it does not directly affect the microwave opacity calculations, it is essential in the development of an accurate model. The calculation of Err_{cond} is given as

$$Err_{cond} = \sqrt{Err_{temp}^2 + Err_p^2 + Err_c^2} \tag{2.47}$$

where Err_{temp}, Err_p and Err_c represents the 2σ uncertainties of the measured opacity resulting from variations in temperature, pressure and concentration respectively. The individual uncertainties are obtained by halving the difference between the maximum and minimum of the modeled opacity. A preliminary model must be obtained in order to operate the model with an upper and lower limit for temperature, pressure and concentration. Since the exact effect of Err_{cond} on the measured opacity and refractivity is unknown at the time of measurement, this error is only taken into account during the data fitting process.

According to Hanley et al. (2009), the 95% confidence measurement uncertainty (Err_{tot}) is given in dB/km as

$$Err_{tot} = \sqrt{Err_{inst}^2 + Err_{diel}^2 + Err_{trans}^2 + Err_{asym}^2} \tag{2.48}$$

Hanley (2008) describes in detail the uncertainty associated with the theoretical computation of refractivity using an ideal resonator. This enables the temperature dependence of the cavity resonator (under vacuum conditions) to be modeled based on the resonator's dimensions.

CHAPTER 3

RESULTS AND MODEL FITTING

The goal of this work has been to develop a model for the opacity of ammonia when pressure-broadened by methane in the 5-20 cm wavelength region. A total of 288 laboratory measurements in the 330-450K temperature range were performed from February through to April of 2012, and the necessary free parameters have been determined to best fit the opacity data. The UHP (Ultra-High Purity) grade ammonia and methane used to take measurements of absorptivity (opacity) and the UHP grade argon used for the dielectric matching process were all provided by Airgas, Inc.

The measurement of absorptivity (opacity) includes first adding ammonia of either 100 or 200 mbar pressure to an evacuated pressure vessel containing a cylindrical cavity resonator at the desired temperature within the range of 330-450K. The absorption spectrum of the gas in the pressure vessel is then pressure-broadened by adding methane to a total pressure of 1, 2 and 3 bars. Measurements of absorptivity and refractivity are made with pure ammonia and again at each addition of methane gas. The chamber is evacuated before the dielectric matching process with argon gas is conducted. The measurements of the pressure-broadened ammonia serve as a basis for the development of the model which will accurately determine the role of methane in the microwave absorption of ammonia. Each of the 288 measurements taken represents a different combination of frequency, mixing ratio, temperature and pressure. The following table illustrates the sets of measurements taken in this work

Table 1. Summary of the Experiments Conducted with the Centimeter-Wavelength System

Experimental Dates	Temperature Range (K)	Nominal Pressure (bar) and {NH_3 concentration (%)}
02/2012	449.3 – 449.7	0.097 {100}, 0.996 {9.77}, 2.002 {4.86}, 3.008 {3.23}
02/2012 – 03/2012	449.6 – 449.8	0.203 {100}, 0.999 {20.28}, 2.006 {10.10}, 3.010 {6.73}
03/2012	374.9 – 375.3	0.100 {100}, 1.000 {10.03}, 2.006 {5.00}, 3.001 {3.34}
03/2012	374.6 – 374.7	0.198 {100}, 1.000 {19.83}, 2.001 {9.90}, 3.017 {6.57}
03/2012 – 04/2012	329.3 – 329.7	0.107 {100}, 0.999 {10.67}, 2.000 {5.33}, 3.006 {3.55}
04/2012	329.6 – 329.8	0.201 {100}, 1.001 {20.08}, 1.998 {10.06}, 3.012 {6.67}

3.1 Data Fitting

A new model for the opacity of ammonia in a methane environment has been developed based on the laboratory measurements obtained with the high-temperature system. The measurements of opacity were made with the cylindrical cavity resonator within the frequency range of 1.5-6 GHz. All 288 measurements were taken with a single consistent system and are given equal weighting in the modeling process.

However, the data points taken at the frequency of 3.09 GHz were noticeably unreliable and inconsistent across all pressures, mixing ratios and concentrations. A test was conducted to determine the root cause of this behavior and it was determined that there is an unusually high level of coupling from the cables to resonance at this frequency. This lack of isolation implies that any small changes in the cable or the dielectric match could greatly affect the opacity results and magnify the associated uncertainties. It is likely that the problem stemmed from a physical movement at the point where the cable was fed into the resonator. Also note that this issue is more noticeable at the lower temperatures of 330K and 375K. Thus these 24 data points were not used in the data fitting process. They are, however, plotted (below) on the graphs illustrating the correlation between microwave absorption and frequencies for the different temperature,

concentration and pressure combinations to determine the model performance. The remaining 264 measurements taken at the other frequencies are deemed reliable and are utilized in the model development process.

The minimizing method of Levenberg-Marquardt (Levenberg, 1944; Marquardt, 1963) was adopted to optimize the fit between the model and the laboratory measurements

$$\chi = \frac{\alpha_{measured} - \alpha_{model}}{Err_{measured}} \tag{3.1}$$

where $\alpha_{measured}$, α_{model} and $Err_{measured}$ are the measured opacity, modeled opacity and measured uncertainty in opacity respectively (all in units of dB/km). Unlike previous work by Devaraj et al. (2011), where each measurement is also assigned a weight to prevent the model from skewing towards the conditions of the most frequent measurements taken, each measurement is given the same weighting because each concentration, pressure and temperature is equally represented in the group of measurements. In the minimizing process, the measured uncertainty in the opacity measurements is given as

$$Err_{measured} = Err_{tot} + Err_{cond} \tag{3.2}$$

where Err_{tot} represents the total uncertainty in opacity and Err_{cond} is the uncertainty as a result of experimental conditions (pressures and temperatures). The uncertainty due to experimental conditions was not considered in the early stages of model optimization. Once a preliminary version of the model was developed, Err_{cond} was calculated and included in the measured uncertainty in opacity; this process was repeated recursively until a convergent solution was found. The uncertainty due to experimental conditions was not a significant contributor to the overall uncertainty, only causing a minor change in the values of the optimized free parameters.

The uncertainty due to experimental conditions has been added to the total uncertainty for each opacity measurements to take into account uncertainties in concentration, temperature and pressure.

The root mean squared value of the χ function was minimized for data across all concentrations, temperatures and pressures in order to determine the free parameters for the best data fit. The formalism for the opacity of ammonia (Hanley et al., 2009) was utilized in this work as a basis for modeling the opacity of ammonia in a high-temperature methane environment. The values for the free parameters used to determine the opacity of pure ammonia are described in Hanley et al. (2009), and the effects of methane broadening of ammonia developed in this work is an extension of this existing formalism for pure ammonia.

Since all the data collected in this work was within the frequency range of 1.5-6 GHz, inversion transitions, rather than rotational or v_2 roto-vibrational transitions, are the main contributor to the measured opacity of ammonia. As a result, only the free parameters for the opacity due to inversion transitions were optimized.

3.2 Ammonia-Methane Mixture Absorption Formalism

The following relationship is used to calculate the opacity of a collisionally broadened gas (Townes and Schawlow, 1955)

$$\alpha = \sum_j A_j \pi \Delta v_j F_j \left(v, v_{(0,j)}, \dots\right) \qquad (cm^{-1}) \tag{3.3}$$

where for line j, A_j is the absorption at the line center (cm^{-1}), Δv_j is the linewidth – half width at half max (cm^{-1}), $F_j\left(v, v_{(0,j)}, \dots\right)$ is the lineshape function. The variable v represents the frequency of the electromagnetic wave that is incident on the gas (cm^{-1}) and $v_{(0,j)}$ is the

frequency at the center of the line (cm^{-1}). The absorption at the line center is calculated with information obtained from the latest JPL catalog as described in Pickett et al. (1998) and is described as

$$A_j = \frac{n\, I_j(T)}{\pi \Delta v_j} \qquad (cm^{-1}) \tag{3.4}$$

where for line j, n is the number density of the gas expressed in $\left(\frac{molecules}{cm^3}\right)$, $I_j(T)$ is the line intensity at temperature T in the units of $\left(\frac{cm^{-1}}{molecules/cm^2}\right)$ and the linewidth parameter, Δv_j, is expressed in cm^{-1}. The number density n of the gas is calculated by the following relationship

$$n = \frac{0.1 \times P_{ideal}}{k_B T} \tag{3.5}$$

where P_{ideal} is the gas's ideal partial pressure expressed in bars, k_B is the Boltzmann's constant (1.38×10^{-23} J/K) and T is the temperature in K. The following relationship is utilized to compute the ideal partial pressure of the gas under investigation

$$P_{ideal} = \frac{\rho R_0 T}{M} \qquad (bars) \tag{3.6}$$

where ρ is the density of the gas in $\left(\frac{g}{m^3}\right)$, R_0 represents the ideal gas constant, T is the temperature in K and M is the molecular mass of the gas expressed in $\left(\frac{g}{mol}\right)$. The ideal gas R_0 constant is taken to be 8.314472×10^{-5} $\left(\frac{g}{mol}\right)$ for all gases in this work. Under the conditions of these experiments, ammonia and methane behaves as ideal gases, and thus the ideal pressures can be determined directly by pressure gauge measurements. The following relationship is utilized to calculate the line intensity at temperature T

$$I_j(T) \approx I_j(T_0)\left(\frac{T_0}{T}\right)^{\eta+1} exp^{\left(\left(\frac{1}{T_0}-\frac{1}{T}\right)E_{(l,j)}\frac{hc}{k_B}\right)} \tag{3.7}$$

where for line j, $I_j(T_0)$ is the line intensity observed at the reference temperature T_0, $E_{(l,j)}$ is the energy associated with the lower state transition (cm^{-1}), c is the speed of light expressed in $\left(\frac{cm}{s}\right)$ and finally, h is the Planck's constant in the units of J·sec. The temperature dependence η is approximately equal to 3/2 for symmetric-top and non-linear molecules such as ammonia; and approximately equal to 1 for linear molecules, as per Townes and Schawlow (1955).

The numerical values for $v_{(0,j)}$, $I_j(T_0)$ and $E_{(l,j)}$ used in the previous equations are obtained from the latest JPL catalog (Pickett et al., 1998) (Version 5, September 2010). In the spectral line catalog, the line intensity at the reference temperature T_0 is provided in the units of $\log_{10}(nm^2MHz)$ and must undergo unit conversions before it is utilized in the calculations. The catalog value is taken as the exponent of 10, followed by dividing the result by 2.99793458×10^{18} in order to be successfully converted into the units of $\left(\frac{cm^{-1}}{molecules/cm^2}\right)$. The linewidth parameter is calculated by the following relationship

$$\Delta v_j = \sum_i v^0_{(i,j)} P_{(i,ideal)}\left(\frac{T_0}{T}\right)^{\xi_{ij}} \qquad (cm^{-1}) \tag{3.8}$$

where for the gas i and line j, $v^0_{(i,j)}$ is the broadening parameter expressed in (cm^{-1}/bar) , $P_{(i,ideal)}$ is the ideal partial pressure of the gas under consideration and lastly, ξ_{ij} is the temperature dependence of the broadening parameter with the following correlation

$$\Delta v_j \propto T^{-\frac{m+1}{2(m-1)}} = T^{-\xi} \tag{3.9}$$

where $1 < m < \infty$ and $m = 3$ is the lower limit for neutral gases. As a result, this yields an allowable range of $0.5 < \xi < 1.0$ (Townes and Schawlow, 1955).

3.3 Line Parameters

The Ben-Reuven lineshape (Ben-Reuven, 1966) was adopted in order to represent the inversion transitions of ammonia, since it best accounts for all of the physical interactions in such transitions. In order to the fully describe the lineshape of the gas, the linewidths need to be known. For ammonia, the self-broadening parameters used are those outlined in Hanley et al. (2009). However, the foreign-gas-broadening parameters for methane were not available since no prior work has been conducted to determine its role in the opacity of ammonia. The free broadening parameters for methane in the modified Ben-Reuven lineshape were optimized and the values which best fit the laboratory opacity measurements of the ammonia-methane mixture were utilized in the formalism developed in this work.

3.4 Formalism of Ammonia Opacity Broadened by Methane

The formalism for the opacity of ammonia broadened by methane is developed based on a modified Ben-Rueven lineshape for the inversion transitions. The total opacity is given by

$$\alpha_{tot} = \alpha_{inv}\ (\text{cm}^{-1}) \times 434294.5 \qquad (\text{dB/km}) \qquad (3.10)$$

where α_{inv} represents the opacity due to inversion transitions and the factor 434294.5 is the unit conversion from cm^{-1} to dB/km. Pure ammonia's opacity due to inversion transitions is modeled with a modified Ben-Rueven lineshape described in Hanley et al. (2009); utilizing the identical values for the self-broadening parameters. The relationship for the opacity due to inversion lines is

$$\alpha_{inv} = \frac{0.1 D_{inv} P_{NH_3}}{k_B T}\left(\frac{2}{\pi}\right)\left(\frac{T_0}{T}\right)^{\eta+1} \times \sum_j \left(I_j(T_0)\, exp^{\left(\left(\frac{1}{T_0}-\frac{1}{T}\right) E_{(l,j)} \frac{hc}{k_B}\right)} \left(\frac{v}{v_{(0,j)}}\right)^2 \right.$$

$$\left. \times \left[\frac{(\gamma_j - \zeta_j)v^2 + (\gamma_j + \zeta_j)\left[(v_{(0,j)} + \delta_j)^2 + {\gamma_j}^2 - {\zeta_j}^2\right]}{\left[v^2 - \left(v_{(0,j)} + \delta_j\right)^2 - {\gamma_j}^2 + {\zeta_j}^2\right]^2 + 4v^2{\gamma_j}^2}\right] \right) \qquad (cm^{-1})$$

(3.11)

where for line j, $v_{(0,j)}$ is the center frequency, γ_j is the linewidth parameter, ζ_j is the coupling parameter, δ_j is the pressure shift parameter and D_{inv} is a unitless scaling factor equal to 0.9301 as determined by Hanley et al. (2009). Each of the variables should be expressed in the unit of cm^{-1}. Note that usually the center frequency, the linewidth parameter, the coupling parameter and the shift parameters are usually in the units of GHz. The unit conversion must be performed before the values can be used to calculate the gas opacity. The linewidth and coupling parameters are calculated by adding the individual contributions of ammonia and methane as follows

$$\gamma_j = \gamma_{CH_4} P_{CH_4} \left(\frac{300}{T}\right)^{\Gamma_{CH_4}} + \gamma_{NH_3} \gamma_{(0,j)} P_{NH_3} \left(\frac{300}{T}\right)^{\Gamma_{NH_3}} \qquad (GHz) \qquad (3.12)$$

$$\zeta_j = \zeta_{CH_4} P_{CH_4} \left(\frac{300}{T}\right)^{Z_{CH_4}} + \zeta_{NH_3} \gamma_{(0,j)} P_{NH_3} \left(\frac{300}{T}\right)^{Z_{NH_3}} \qquad (GHz) \qquad (3.13)$$

where for gas i (i = CH_4 and NH_3) and line j, γ_i and ζ_i represent the scaling terms, Γ_i and Z_i are the temperature dependences for the broadening gas, P_i denotes the pressure of the gas in bars, and $\gamma_{(0,j)}$ is the self-broadening linewidths of ammonia expressed in MHz/Torr. The unit conversion of ammonia's self-broadening linewidths into GHz/bar is taken into account through the constants γ_{NH_3} and ζ_{NH_3} for the linewidth and coupling parameters respectively. Whereas γ_{NH_3} is equal to 0.852 and ζ_{NH_3} is equal to 0.5296, the exponents Γ_{NH_3} and Z_{NH_3} are assigned the

values of 1 and 1.554 respectively (see Hanley et al., 2009). The calculations of $\gamma_{(0,j)}$ are obtained from Poynter and Kakar (1975), using 295K as the reference temperature, T_0. The following expression is used to calculate the self-broadening linewidths for lines that occur at frequencies less than 7.2 GHz and $J > 16$, where J is the ammonia molecule's total angular momentum vector

$$\gamma_0(J,K) = 25.923 \frac{K}{\sqrt{J(J+1)}} \qquad \left(\frac{MHz}{Torr}\right) \tag{3.14}$$

where K is the projection of J on the molecular axis of ammonia. Finally, the pressure shift parameter, δ_j, is computed as

$$\delta_j = \mathrm{d} \times \gamma_j \qquad (GHz) \tag{3.15}$$

where d is an empirically derived constant equal to -0.0498 as determined by Hanley et al. (2009). The optimized free parameters for methane's scaling parameters and temperature dependences for both the linewidth and coupling parameters are derived through fitting the model to the laboratory results. Ammonia's self-broadening free parameters for the linewidth and coupling parameters are described in Hanley et al. (2009) and are also displayed in the following table along with methane's broadening free parameters

Table 2. Constants for the New Microwave Opacity Model of CH_4-broadened NH_3

	$i = CH_4$	$i = NH_3$
γ_i	2.15	0.852
Γ_i	1	1
ζ_i	1.02	0.5296
Z_i	1	1.554
d = -0.0498		D_{inv} = 0.9301

This new model for the opacity of ammonia pressure-broadened by methane in the 5-20 cm wavelength range is fitted to the measurements of up to 3 bars and a temperature range of 330 to 450K. The latest spectral lines information in the JPL catalogue (Pickett et al., 1998) and a functional software model in MATLAB are made available online at the Planetary Atmospheres Laboratory at Georgia Tech website.

3.5 Model Performance

In Figures 3-26, the model for the opacity of ammonia pressure-broadened by methane is plotted along with the opacity measurements taken in the laboratory. All 288 measurements taken in the 330-450K temperature region at pressures of up to 3 bars (including either 100 mbar or 200 mbar of ammonia) made in this work were used to evaluate the performance of the model in the 1.5-6 GHz range.

The error bars of each data point displays the 2σ total uncertainties and uncertainty due to experimental conditions. The Hanley ammonia model was selected as the basis of the methane pressure-broadening formalism because it best fits the pure ammonia opacity measurements collected in this work. However from initial observations, it appears that the model consistently understate the opacity measurements of pure ammonia across the temperatures of 330K and 375K. The formalism for methane is an extension of this model, therefore, it is also important to note that the methane foreign-gas-broadening terms of the linewidth and coupling parameters may have overstated the effects of methane at lower pressures.

Plotting the model with opacity measurements provides a suitable method to visually and quantitatively assess the quality of the model. The formalism accurately models 84.72% of all data points within the 2σ uncertainty, which is represented by the error bars. If the problematic

opacity measurements at 3.09 GHz are disregarded, the model matches up to 91.41% of the laboratory opacity measurements within the 2σ uncertainty.

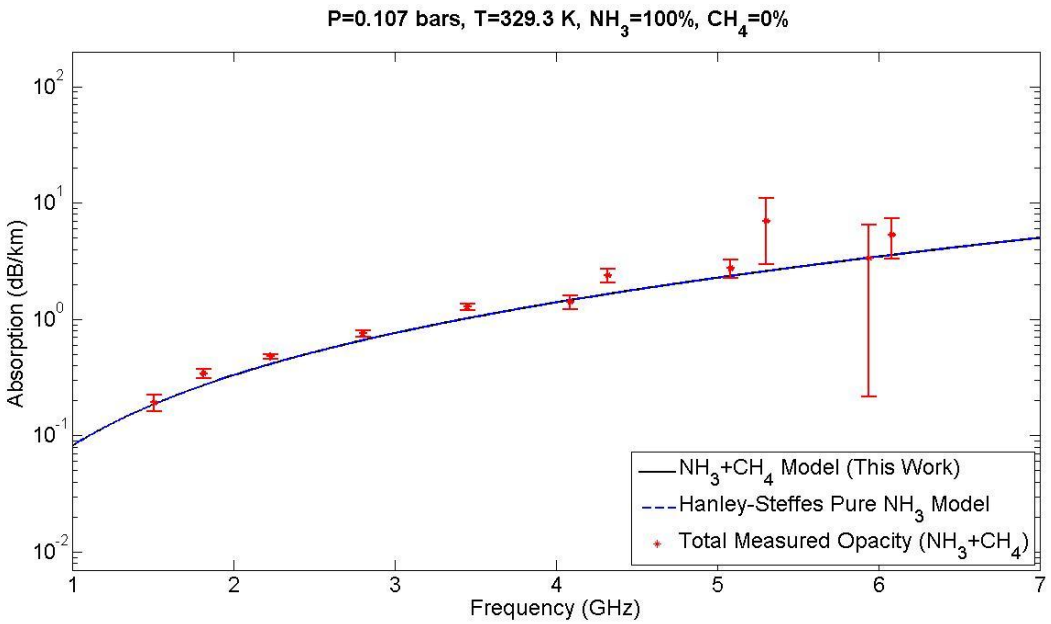

Figure 3: Experiment at 330K with 100 mb of pure ammonia.

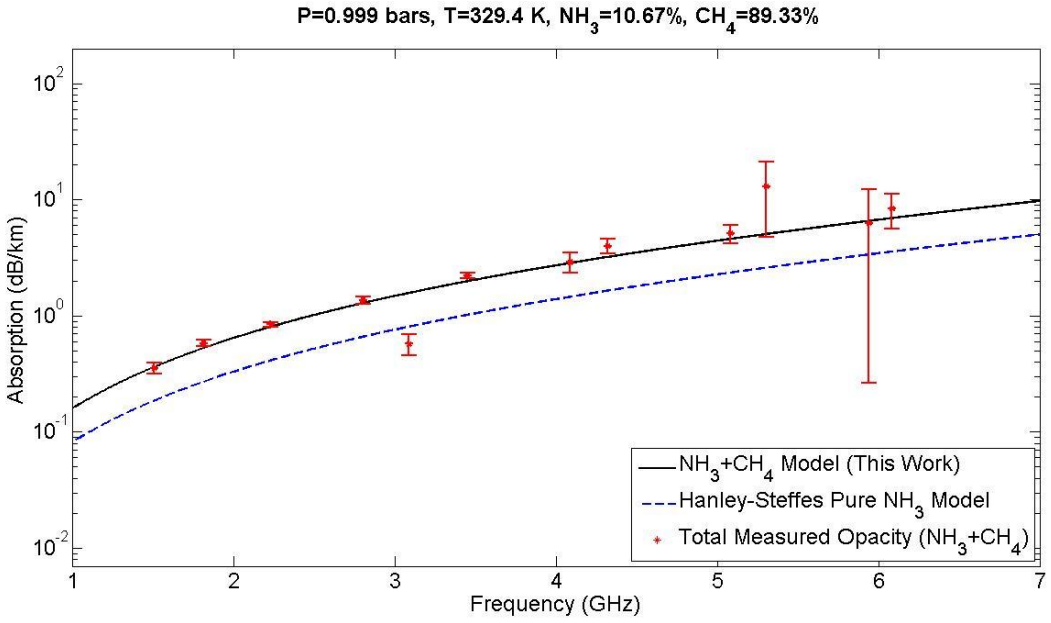

Figure 4: Experiment at 330K with 100 mb of ammonia pressure-broadened by methane to 1 bar of total pressure.

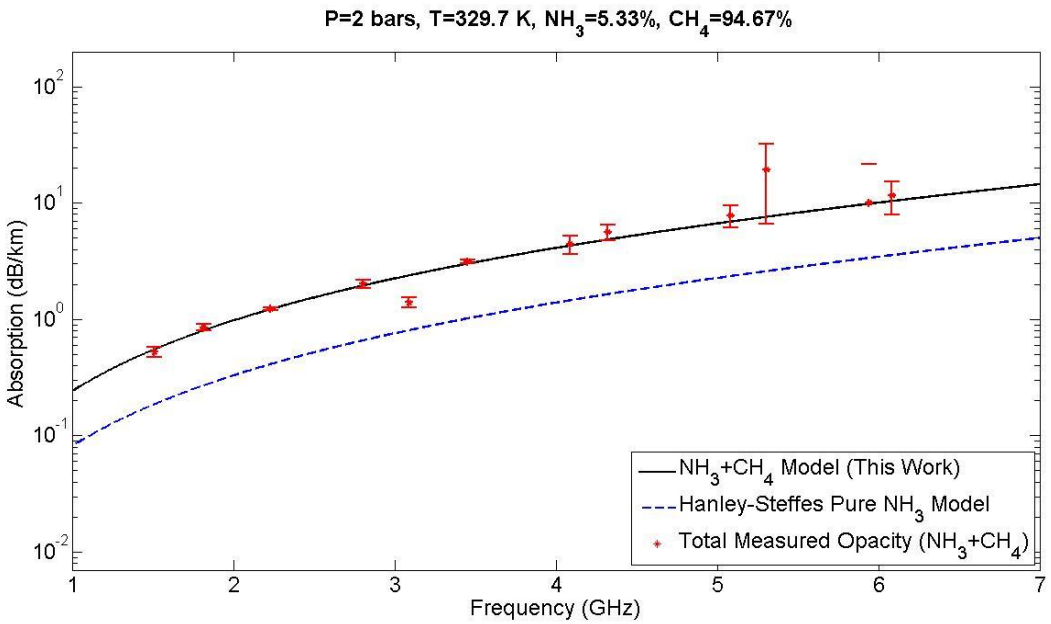

Figure 5: Experiment at 330K with 100 mb of ammonia pressure-broadened by methane to 2 bars of total pressure.

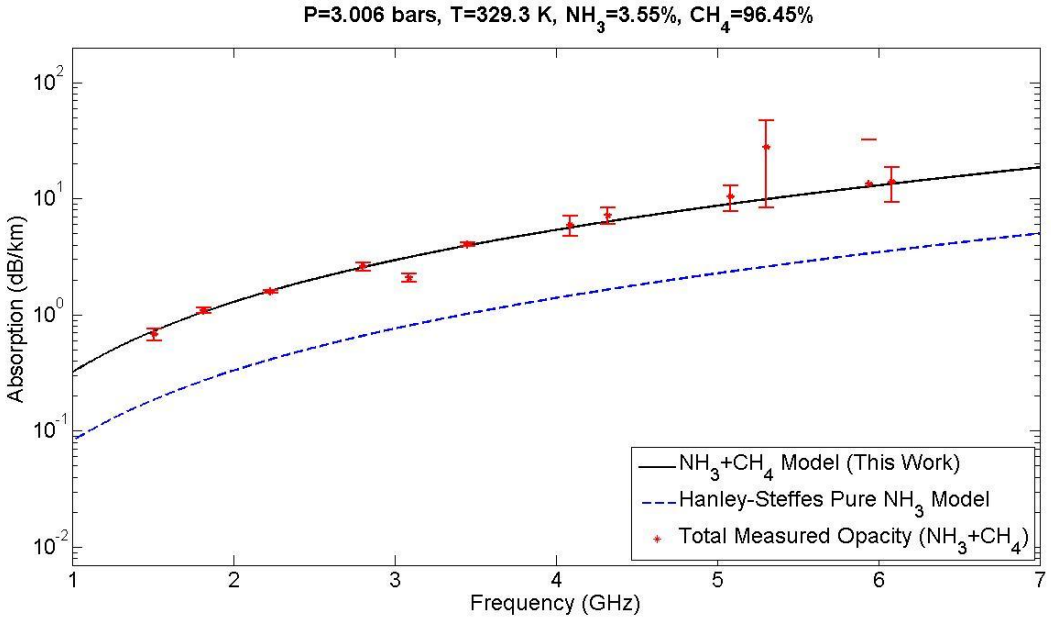

Figure 6: Experiment at 330K with 100 mb of ammonia pressure-broadened by methane to 3 bars of total pressure.

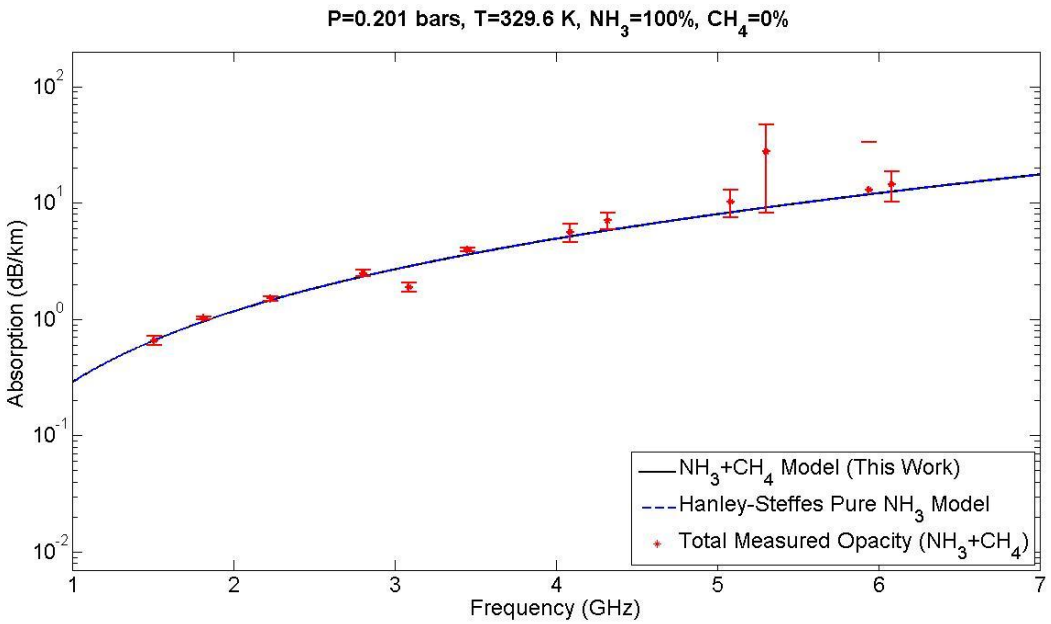

Figure 7: Experiment at 330K with 200 mb of pure ammonia.

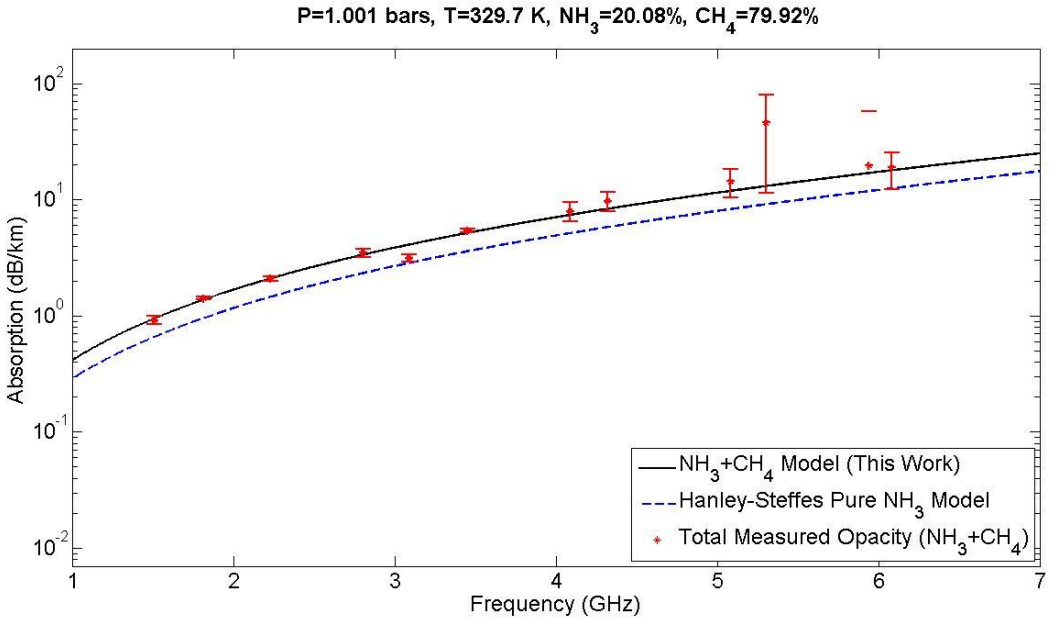

Figure 8: Experiment at 330K with 200 mb of ammonia pressure-broadened by methane to 1 bar of total pressure.

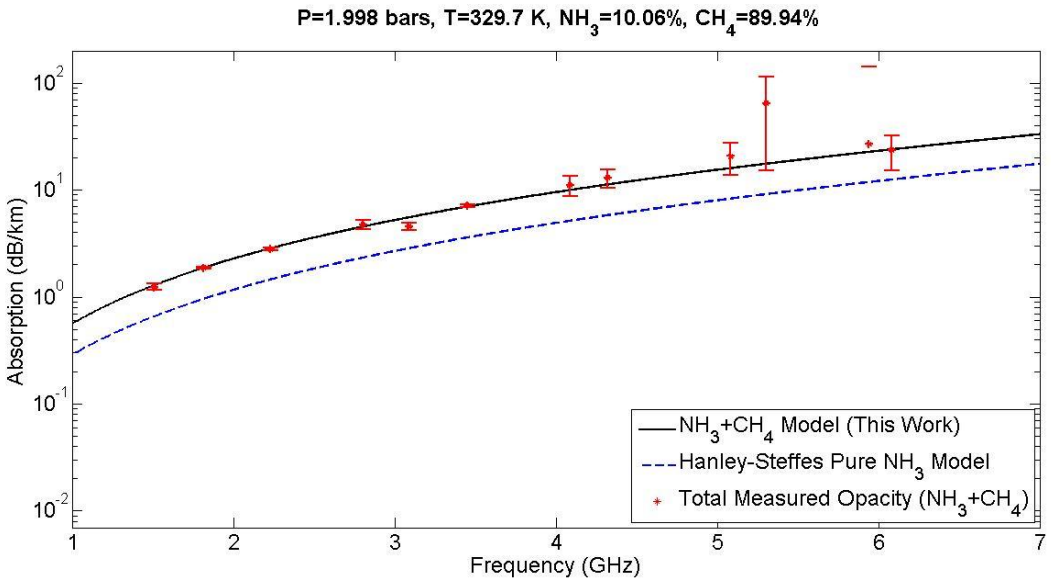

Figure 9: Experiment at 330K with 200 mb of ammonia pressure-broadened by methane to 2 bars of total pressure.

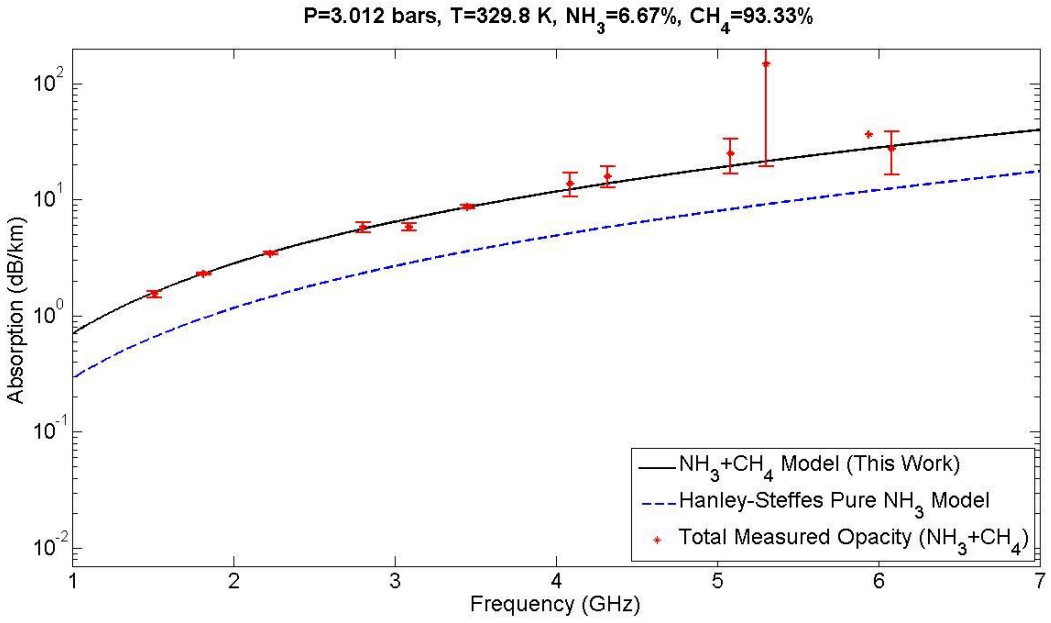

Figure 10: Experiment at 330K with 200 mb of ammonia pressure-broadened by methane to 3 bars of total pressure.

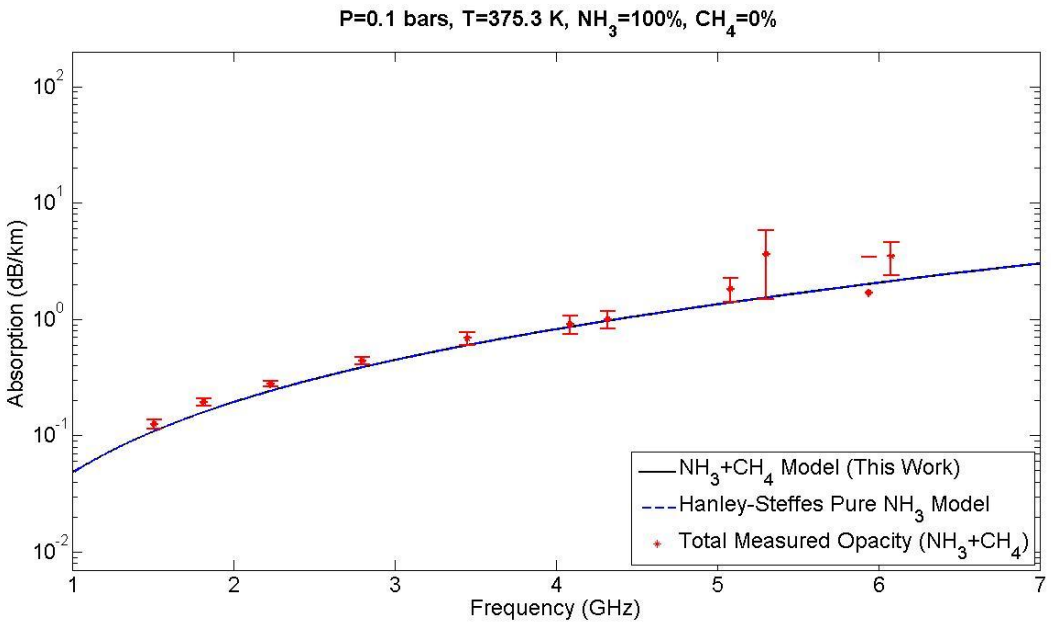

Figure 11: Experiment at 375K with 100 mb of pure ammonia.

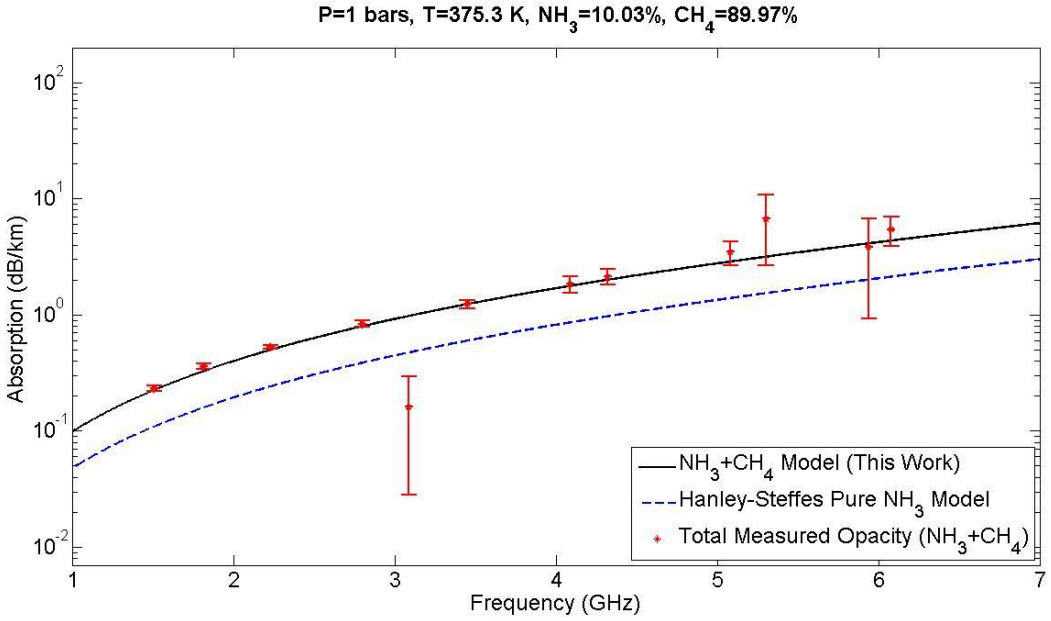

Figure 12: Experiment at 375K with 100 mb of ammonia pressure-broadened by methane to 1 bar of total pressure.

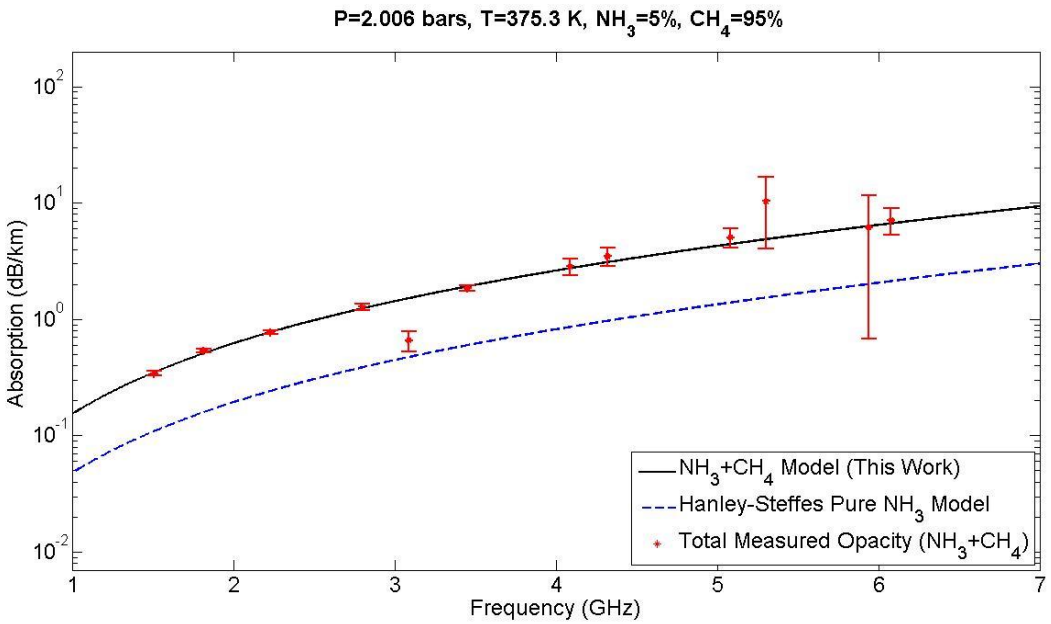

Figure 13: Experiment at 375K with 100 mb of ammonia pressure-broadened by methane to 2 bars of total pressure.

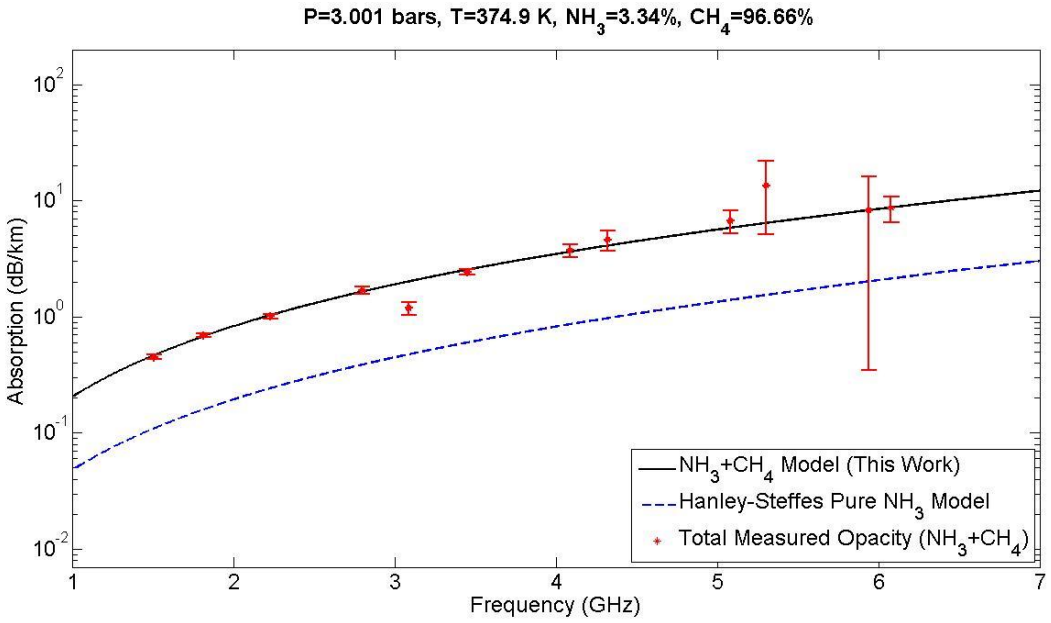

Figure 14: Experiment at 375K with 100 mb of ammonia pressure-broadened by methane to 3 bars of total pressure.

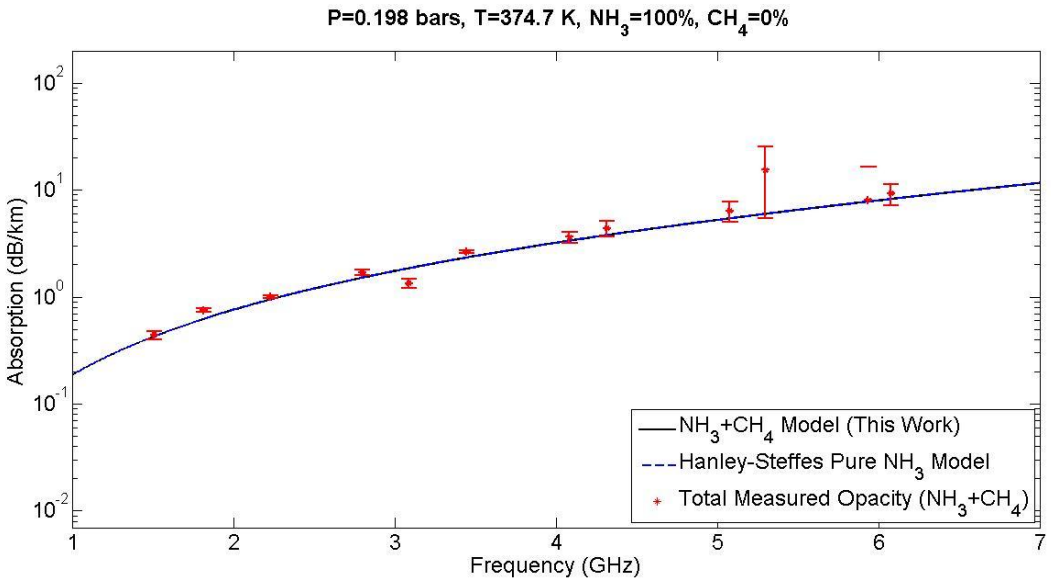

Figure 15: Experiment at 375K with 200 mb of pure ammonia.

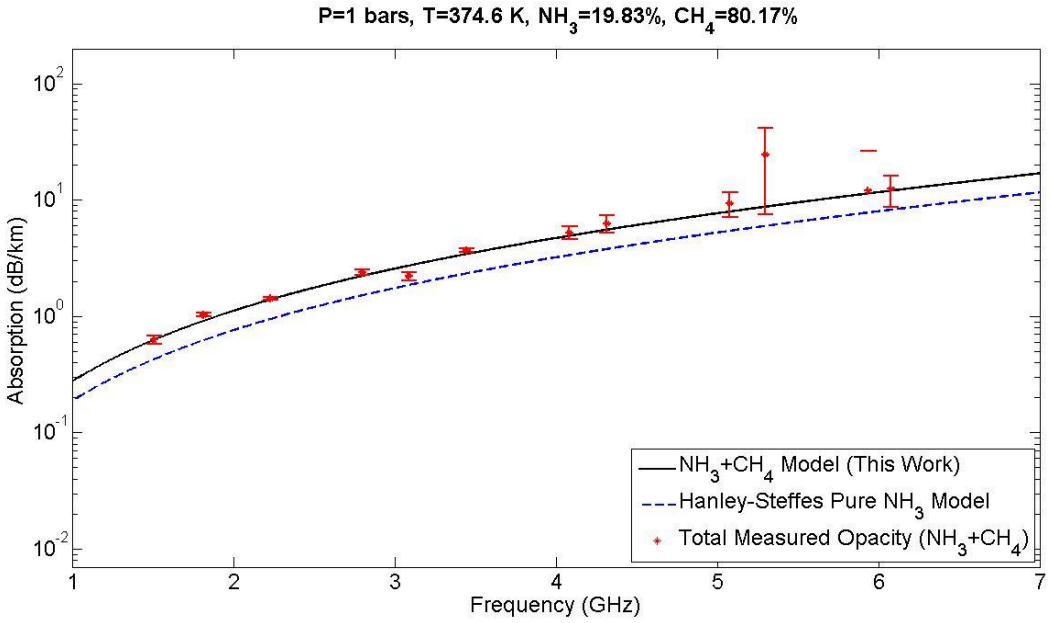

Figure 16: Experiment at 375K with 200 mb of ammonia pressure-broadened by methane to 1 bar of total pressure.

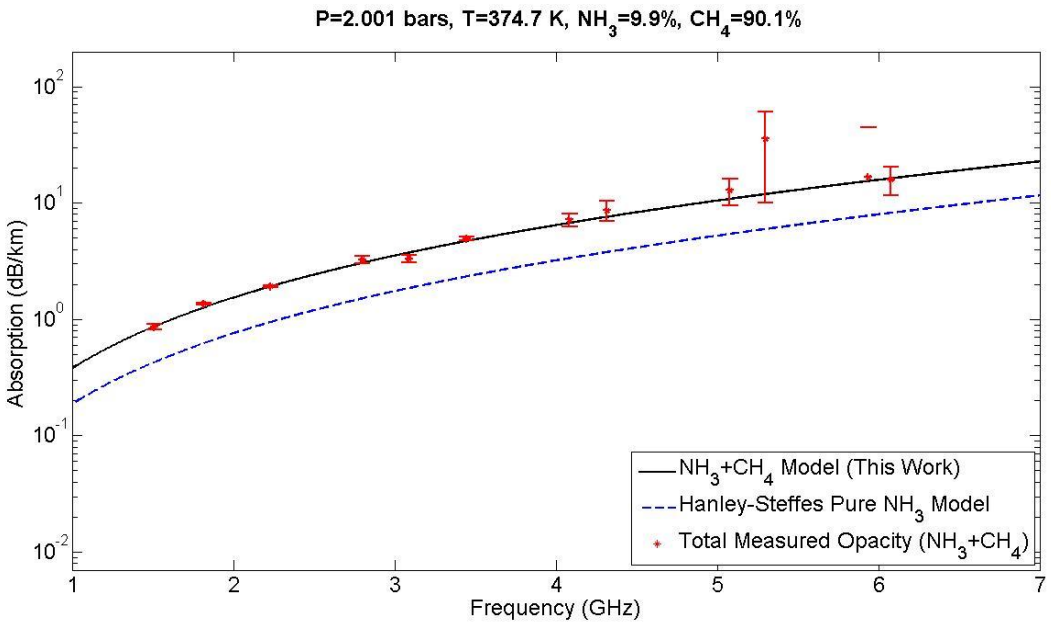

Figure 17: Experiment at 375K with 200 mb of ammonia pressure-broadened by methane to 2 bars of total pressure.

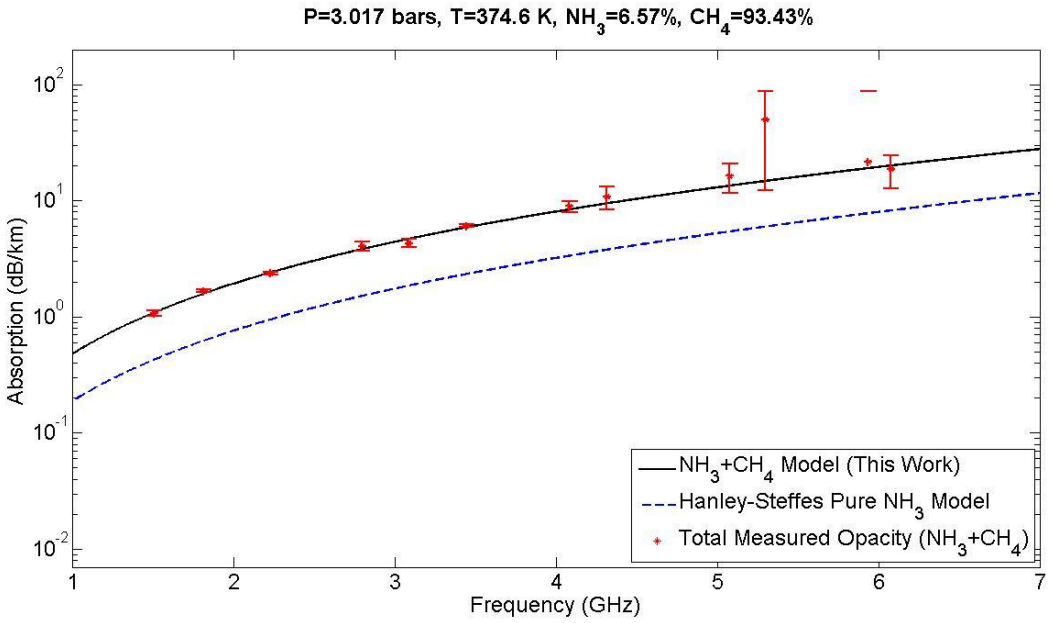

Figure 18: Experiment at 375K with 200 mb of ammonia pressure-broadened by methane to 3 bars of total pressure.

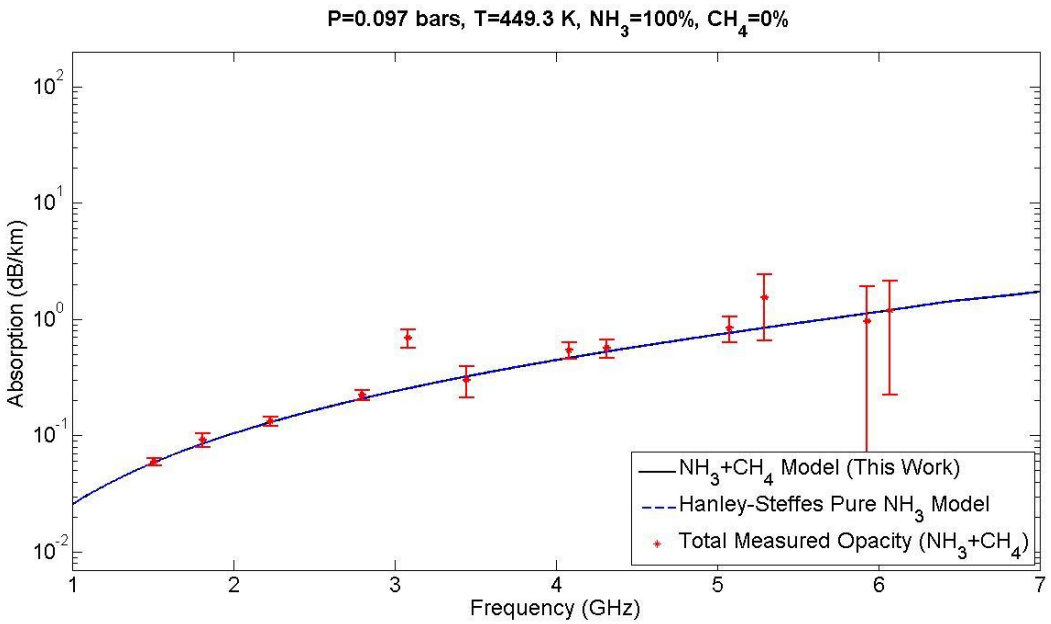

Figure 19: Experiment at 450K with 100 mb of pure ammonia.

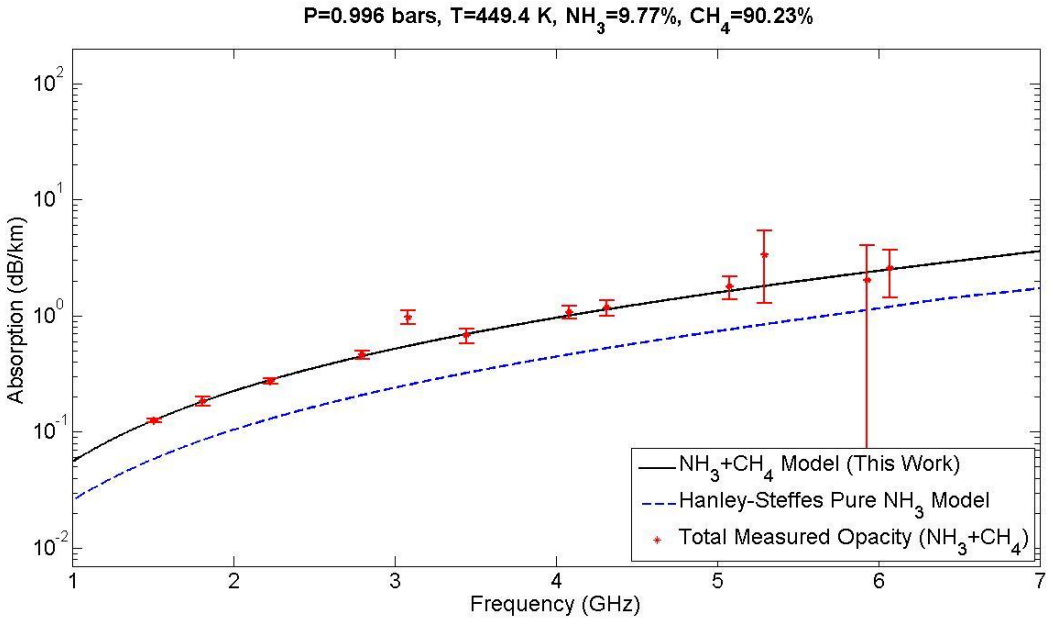

Figure 20: Experiment at 450K with 100 mb of ammonia pressure-broadened by methane to 1 bar of total pressure.

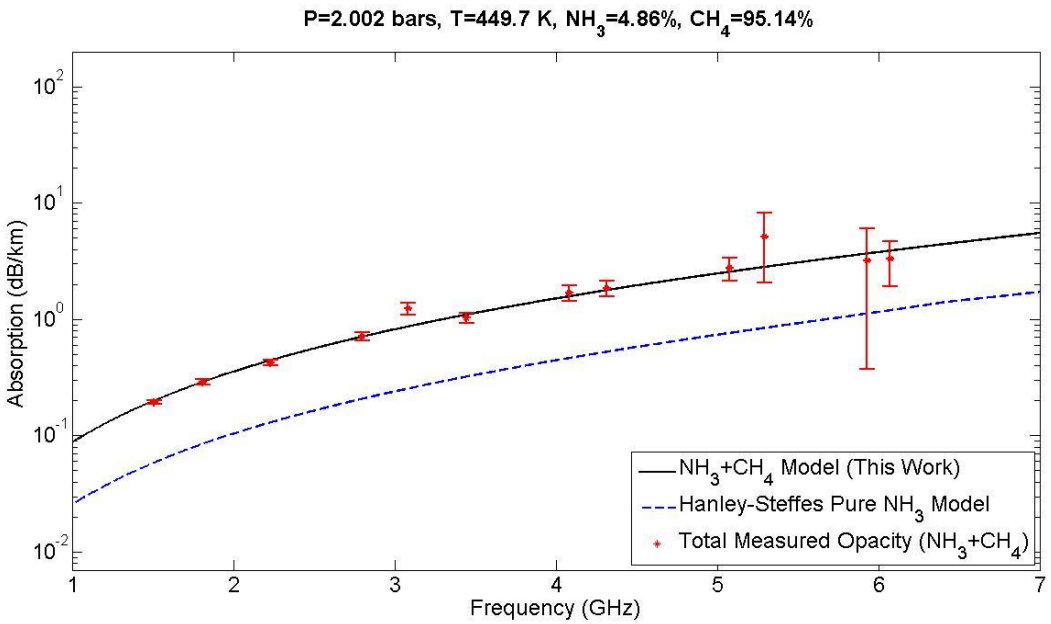

Figure 21: Experiment at 450K with 100 mb of ammonia pressure-broadened by methane to 2 bars of total pressure.

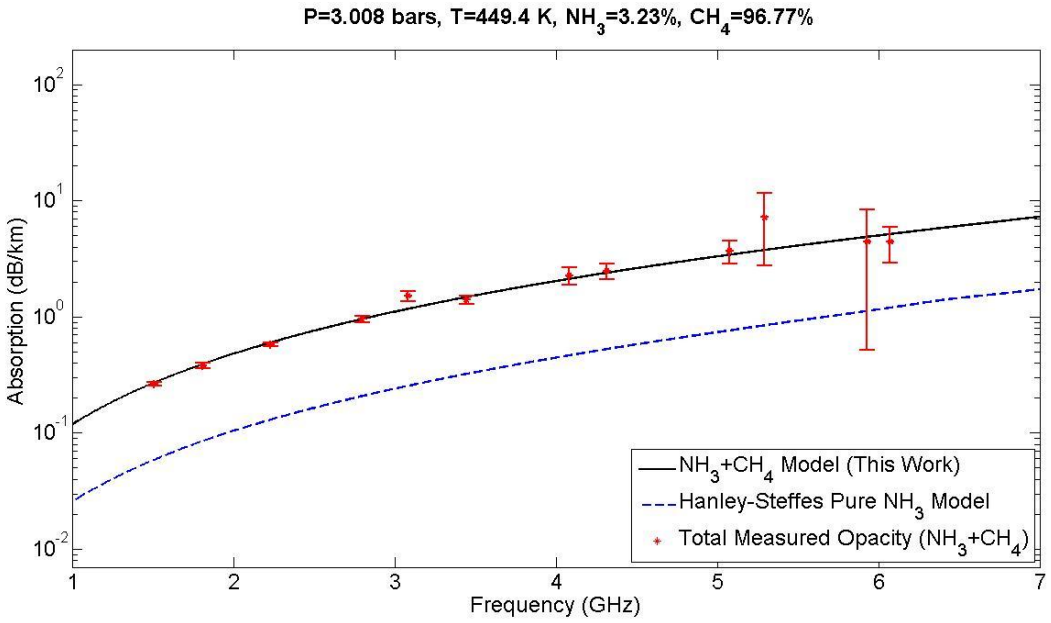

Figure 22: Experiment at 450K with 100 mb of ammonia pressure-broadened by methane to 3 bars of total pressure.

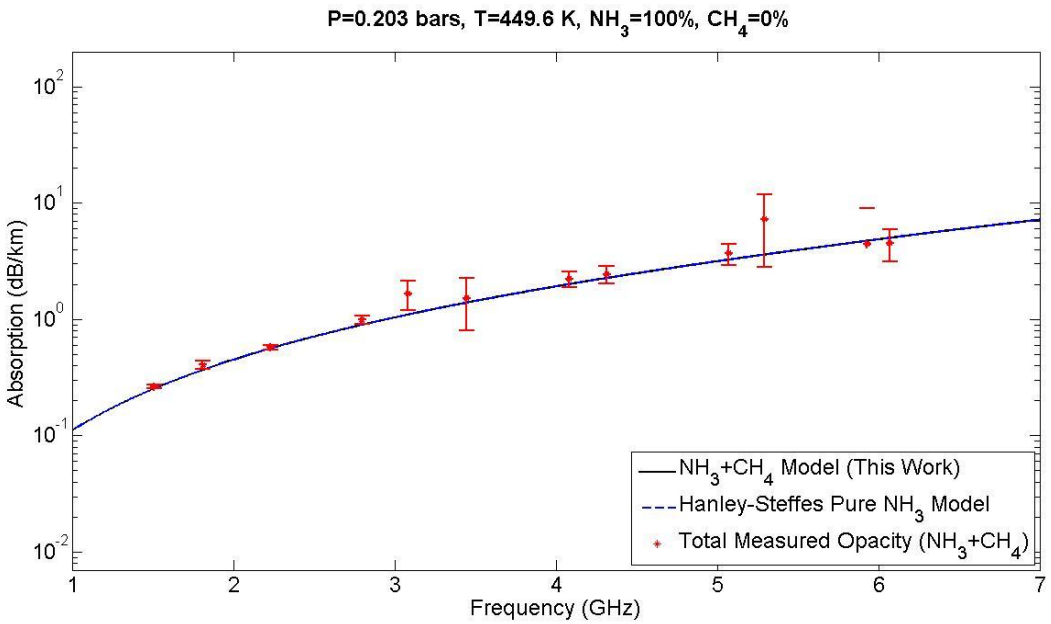

Figure 23: Experiment at 450K with 200 mb of pure ammonia.

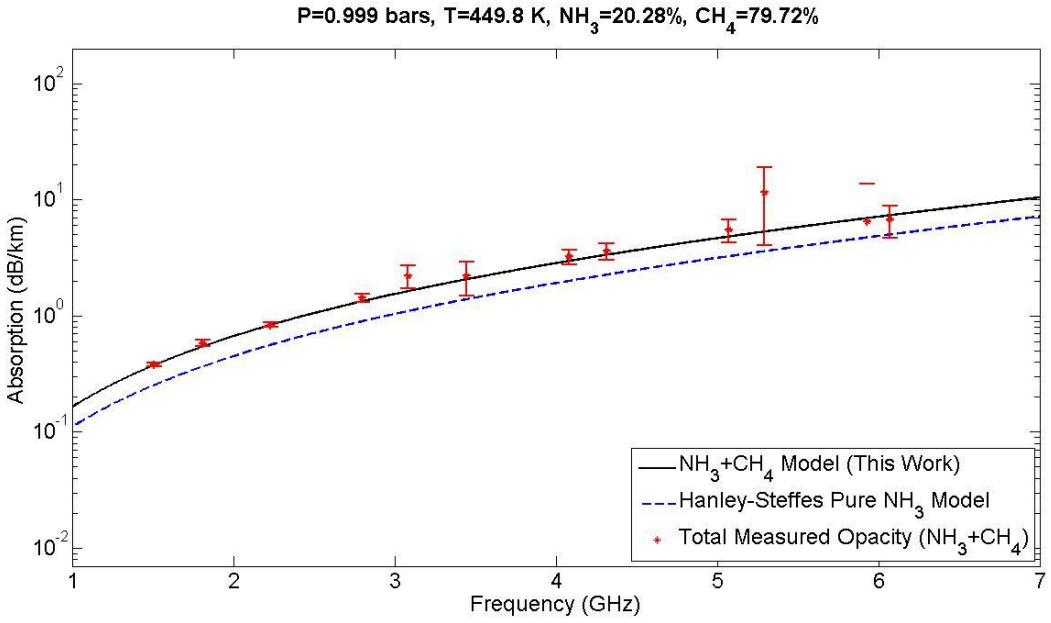

Figure 24: Experiment at 450K with 200 mb of ammonia pressure-broadened by methane to 1 bar of total pressure.

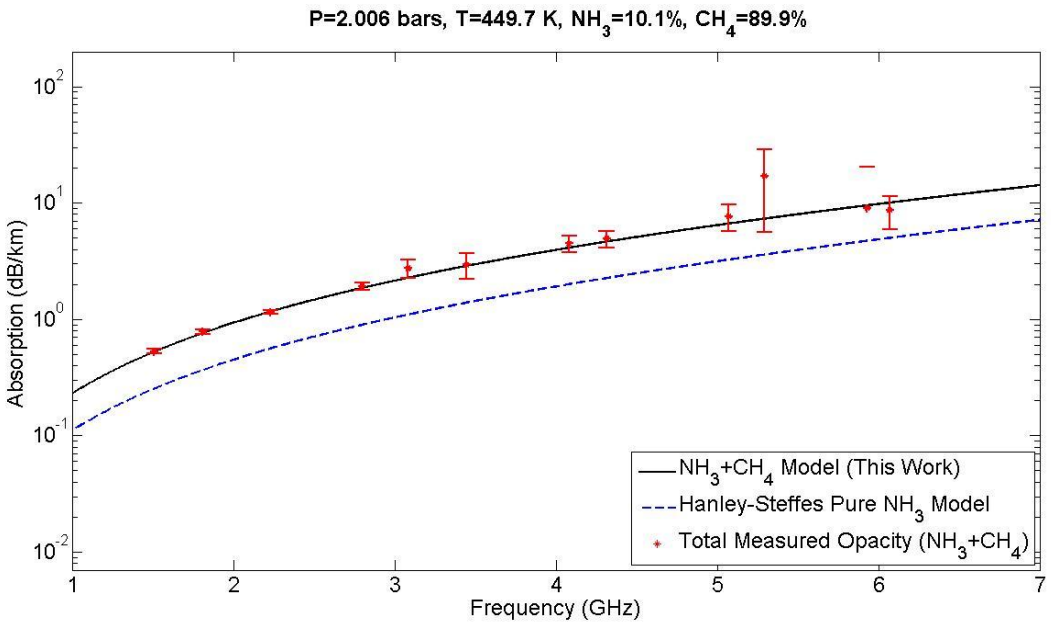

Figure 25: Experiment at 450K with 200 mb of ammonia pressure-broadened by methane to 2 bars of total pressure.

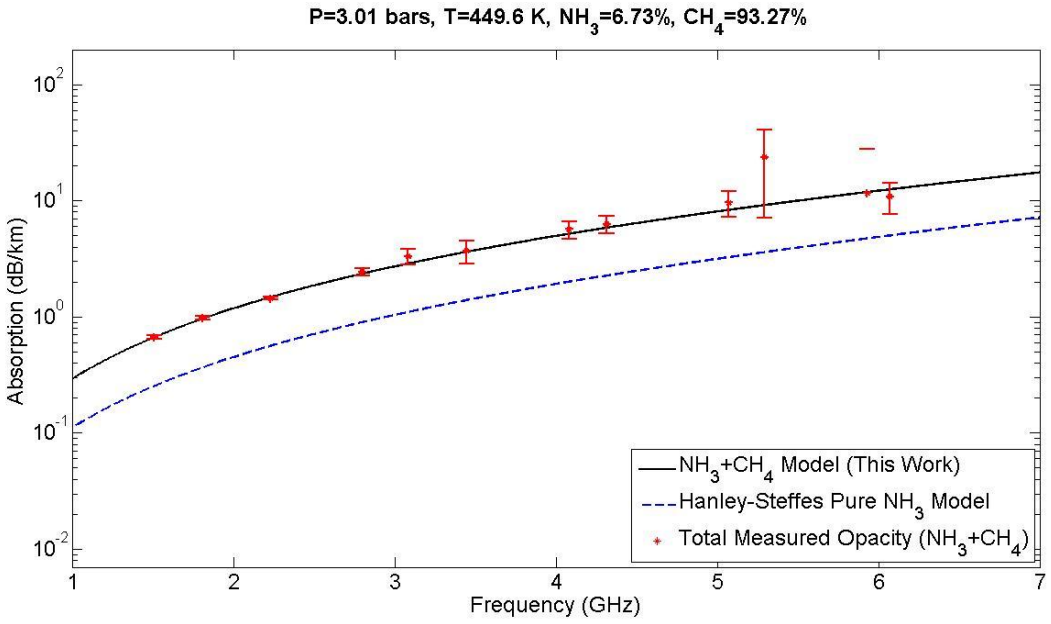

Figure 26: Experiment at 450K with 200 mb of ammonia pressure-broadened by methane to 3 bars of total pressure.

CHAPTER 4

SUMMARY AND CONCLUSIONS

The objective of this research has been to better understand the microwave opacity of ammonia when pressure-broadened by methane in the centimeter-wavelength region. As part of this work, 288 laboratory measurements were collected using the Georgia Tech high-pressure and high-temperature planetary atmospheric simulator. Experiments were conducted using pure ammonia and an ammonia-methane mixture in the 5-20 cm wavelength range. Data was collected using either 100 or 200mb of ammonia pressure-broadened by 1 to 3 bars of methane in the 330K to 450K temperature range. An existing model for the microwave opacity of pure ammonia (Hanley et al, 2009) served as a basis for the development of the model for the opacity of ammonia pressure-broadened by methane, as described in this work. The resulting model was developed based on the collected data and provides a good fit with the experimental data (successfully fitting up to 91.41% of the reliable results within 2σ uncertainty). The use of the model beyond the measured temperatures (330-450K), frequencies (1.5-6 GHz), and ammonia concentrations utilized in this laboratory work will likely give accurate results, since the model is based on the highly robust Ben-Reuven lineshape (see, e.g, Hanley et al., 2009 or Devaraj 2011). From the results obtained, it is concluded that the pressure-broadening of the ammonia absorption spectrum by methane will not significantly affect the microwave emission spectrum of Jupiter. Thus, this work will enable the MWR team of the Juno mission to more reliably interpret the centimeter-wavelength emission spectrum of Jupiter as seen by the Juno MWR when it arrives at Jupiter in 2016. An additional experiment sequence was conducted at 295K using 40 bars of methane pressure-broadened by 40 bars of hydrogen to ensure that the effects measured were

only due to methane broadening and not its own intrinsic absorption. This work also confirms the microwave transparency of methane in the centimeter-wavelength region.

4.1 Application to Juno

As part of the Juno mission work, updated models for the microwave opacity of ammonia and water vapor have been developed by Hanley et al. (2009) and Karpowicz and Steffes (2011), respectively. Additionally, Devaraj (2011) has shown that the existence of other minor constituents in the atmosphere can affect the absorption spectrum of ammonia through "broadening". Even though methane is a minor constituent in the atmosphere of Jupiter (~0.2% by volume), it is essential to recognize and understand its effects on the absorption behavior of ammonia. The influence of methane on the ammonia absorption spectrum was studied in the laboratory for the first time as part of this research. Prior to this work, no model for the opacity of ammonia broadened by methane existed. This new model, therefore, provides essential information for the Juno MWR team as they interpret the Juno MWR measurements, especially in the accurate retrieval of the atmospheric abundance of ammonia.

Although the presence of methane increases the centimeter-wavelength microwave opacity of ammonia below 23 GHz, its effect is quite small at Jupiter since the relative abundance of methane is low. However, at other jovian planets where methane plays a more dominant role, such as Uranus and Neptune, the broadening effects of methane should be pursued as discussed below. Also of importance to both the Juno mission and to observations of other jovian planets, the additional measurement involving methane and hydrogen confirms the previous laboratory measurements made by Jenkins and Steffes (1988) indicating that methane is microwave transparent at centimeter-wavelengths.

4.2 Suggestions for Future Work

Uranus and Neptune are very similar in their chemical compositions to Jupiter and Saturn, but different in that even though hydrogen and helium remain the most abundant constituents in their planetary atmospheres, both Uranus and Neptune contain a higher proportion of "ices" (which includes water, ammonia and methane) than the other gas giants, Jupiter and Saturn. The third most abundant constituent in the atmosphere of Uranus is methane (~2.3%). Due to this large abundance, the ammonia broadening effects of methane in the centimeter-wavelength region will certainly be more significant and noticeable at Uranus than at Jupiter. The findings of this research will change the way we interpret ground-based and spacecraft-based observations of Uranus. Similarly, Neptune is another icy giant that is highly abundant in methane (2-4%), the third most abundant gas in its atmosphere. In fact, the planet appears blue because the methane in the outer region of its atmosphere absorbs the longer wavelengths of sunlight and reflects the wavelengths that correspond to the color blue in the visible spectrum. The ammonia broadening effects of methane at Neptune will be far more significant in comparison to level expected to be measured by the Juno MWR at Jupiter. Again, this new model for the opacity of ammonia pressure-broadened by methane should be applied to the observations for Uranus and Neptune in order to recognize the extent this finding changes our understanding of methane's role at these "ice" giants.

A laboratory experiment measuring the opacity of hydrogen sulfide in a hydrogen atmosphere is currently being undertaken with the Georgia Tech planetary atmospheric simulator system. The purpose of conducting this sequence of experiment is to ensure that the model for hydrogen sulfide opacity described in DeBoer et al. (1994) yields reliable results at high pressures and temperatures characteristic of the deep atmosphere of Jupiter. It is essential that the Juno mission

team be assured that the microwave opacity from hydrogen sulfide will not compromise the retrievals of water vapor and ammonia to be measured by the Juno MWR.

APPENDIX A - The Opacity of Methane

Another set of laboratory measurements was collected with the objective of determining the microwave opacity of methane in the 5-20 cm wavelength region at the temperature of 295K. For this experiment, methane itself is the test gas. It was further pressure-broadened by hydrogen in the high-pressure outdoor system. This set of laboratory experiments was performed from May through to June of 2012. Similar to the ammonia broadening experiment, the gas bottles were provided by Airgas, Inc. The methane and hydrogen used in the absorptivity measurements were of UHP (Ultra-High Purity) grade as was the argon used for the dielectric matching process.

The measurement of absorptivity (opacity) began by adding 40 bars of methane to the evacuated pressure chamber containing the cylindrical cavity resonator. At the desired temperature of 295K, the opacity measurements were collected. This gas was then pressure-broadened by 40 bars of hydrogen, bringing the total pressure to 80 bars within the resonator. The second set of measurements was taken of the methane-hydrogen mixture at the temperature of 295K. A vacuum was then drawn in the pressure vessel containing the resonator. Argon was then added to match the refractive index of the pure methane at 40 bars. Since it is also a microwave transparent gas, additional hydrogen gas was added to dielectrically match the measurements of the methane-hydrogen mixture taken at 80 bars. As discussed below, the opacity measurements taken in this experiment confirmed the microwave transparency of methane.

A total of 24 measurements were collected; 12 of pure methane at the pressure of 40 bars and another 12 of the methane-hydrogen mixture at the pressure of 80 bars.

Methane Microwave Opacity Data Collection

The software that automates the search for resonances used in our measurements automatically determines the peak frequency of each resonance. Since methane is so refractive, the peak

frequencies of the resonances shifted to dramatically lower frequencies as the gas was added. The shifted location of the peak can be predicted by taking into account the refractivity of the gas mixture as outlined in Hanley and Steffes (2007).

This was the first experiment conducted using such a highly-refractive gas (methane) with the current outdoor high-pressure system. The 40-bar-increment was the largest single step in pressure, and it proved difficult for the software to track the large drop in the center frequencies of each resonance. Subsequently, in order to guide the experimenter to add the right amount of dielectric matching gas, the software must be able to locate the shifted first resonance and indicate whether to add or remove reference gas to bring it to the same frequency as that when the test gas mixture was being measured. Initially, the shift in the peak frequency of the resonances caused them to be located outside the searchable scope of the existing software. As a result, the search range was increased immensely for the software to detect the desired resonance. Once the first resonance is detected, the software automatically searches and takes the measurements for the first five resonances. It then prompts for user inputs to locate the remaining resonances. This shift in the resonances poses the hazard of the software automatically detecting and taking measurements of nearby (undesired) resonances. For example, according to Hanley (2008), the resonances TE(0,1,3) and TE(1,2,2) of the cylindrical cavity resonator are only on the order of 100 MHz apart and a dramatic shift in center frequencies can easily confuse the software in this case.

The method to successfully ensure that the correct resonances have been detected is to compare the predicted and actual peak frequencies of each resonance. The calculation of the predicted shifted center frequency required both the refractive indices of methane and hydrogen. The

normalized refractivity of methane is derived from Spilker (1990) and the normalized refractivity of hydrogen is obtained from Essen (1953). The values used in the calculations are

$N'_{CH_4} = 1.72 \times 10^{-17}$ N-units cm^3 $molecule^{-1}$ and

$N'_{H_2} = 5.06 \times 10^{-18} \pm 1.49 \times 10^{-21}$ N-units cm^3 $molecule^{-1}$

Once the shifted center frequencies were calculated, they were compared to actual ones detected by the network analyzer to verify that the correct resonances are indeed measured. If this was not the case, the network analyzer was manually tuned to locate the appropriate resonances.

The two pressure gauges of the centimeter-wavelength system are only capable of handling pressure measurements of up to 2 bars and 20 bars respectively. This experiment was conducted at the pressures of up to 40 bars of pure methane and 80 bars of the methane-hydrogen mixture. Therefore, the pressure transducer was utilized in determining the total pressure within the pressure vessel for both loaded and matched measurements. The mass flow meter was instrumental in determining the amount of gas needed to achieve the desired total pressure for the loaded case and obtain a match in the peak frequencies for the matching case.

Methane Microwave Opacity Results

The microwave opacity of pure methane and methane pressure-broadened by hydrogen are displayed in Table 3 and Table 4 below respectively. As expected, it appears that methane is extremely transparent. The opacity of methane across the 12 frequencies is not statistically significant. The upper limit for the absorptivity results are calculated by taking into account the 2σ uncertainty of absorption. Even when methane is pressure-broadened by 40 bars of hydrogen, the mixture remained very transparent. From these results, it is clear that methane is not an

opaque gas and its high refractive index makes it a suitable dielectric-matching agent for future experiments. Additionally, methane's transparency indicates that it will not affect the microwave emissions measured by the NASA/Juno Mission Microwave Radiometer (MWR) at Jupiter.

Table 3. The Absorption of Pure Methane and its 2σ Uncertainties at the Respective Center Frequencies

Center Frequency (GHz)	Absorption (dB/km)	2σ Uncertainty of Absorption (dB/km)	Upper Limit (dB/km)
1.4849	-0.0418	0.05417	0.033597
1.7852	-0.0549	0.09096	0.126596
2.1962	-0.0218	0.05642	0.08965
2.7576	-0.0004	0.11504	0.228918
3.0399	-0.4726	0.46845	0.464194
3.3959	-0.0335	0.45772	0.881919
4.0229	-0.1288	0.19697	0.255788
4.2518	-0.2205	0.31498	0.409156
5.0021	-0.1487	0.65998	1.171127
5.2194	-0.3845	0.38551	0.332237
5.8468	0.07382	0.39782	0.645721
5.9855	-0.4681	1.55485	2.63271

Table 4. The Absorption of the Methane-Hydrogen Mixture and its 2σ Uncertainties at the Respective Center Frequencies

Center Frequency (GHz)	Absorption (dB/km)	2σ Uncertainty of Absorption (dB/km)	Upper Limit (dB/km)
1.4776	-0.1418	0.18798	0.070936
1.7764	-0.1242	0.15914	0.175947
2.1854	-0.0298	0.04274	0.051405
2.744	0.03644	0.18032	0.396851
3.0249	0.00688	0.41483	0.836497
3.3792	-0.1515	0.58868	1.025798
4.0031	-0.1583	0.18003	0.14976
4.2309	-0.1559	0.27991	0.40037
4.9775	0.03749	0.4045	0.846399
5.1937	0.00192	0.40723	0.810677
5.9561	-0.1729	3.95987	7.740521

The tabulated results also display the overall 2σ uncertainties of the microwave opacity measurements. The total uncertainty, Err_{tot}, takes into account contributions from asymmetry, dielectric matching, transmissivity and instrumental uncertainties. Note that the data taken at 5.95 GHz of the methane-hydrogen mixture was not included in the results. The presence of a large uncertainty due to asymmetry indicates that there was interference from an undesired nearby resonance.

REFERENCES

Ben-Reuven, A. (1966), Impact broadening of microwave spectra, *Phys. Rev., 145,* 7-22.

DeBoer, D. R., and P.G. Steffes (1994), Laboratory measurements of the microwave properties of H_2S under simulated Jovian conditions with an application to Neptune, *Icarus, 109,* 352-366, doi:10.1006/icar.1994.1099.

DeBoer, D. R., and P. G. Steffes (1996), The Georgia Tech high sensitivity microwave measurement system, *Astrophysics and Space Science, 236,* 111-124.

Devaraj, K. (2011), The centimeter- and millimeter-wavelength ammonia absorption spectra under jovian conditions. Ph.D. thesis, Georgia Institute of Technology.

Devaraj, K., P.G. Steffes, and B. M. Karpowicz (2011), Reconciling the centimeter- and millimeter-wavelength ammonia absorption spectra under jovian conditions: Extensive millimeter-wavelength measurements and a consistent model. *Icarus, 212,* 224-235.

Essen, L. (1953), The Refractive Indices of Water Vapour, Air, Oxygen, Nitrogen, Hydrogen, Deuterium and Helium, *Proceedings of the Physical Society B, 66,* 189-193.

Hanley, T.R. (2008), The microwave opacity of ammonia and water vapor: Application to remote sensing of the atmosphere of Jupiter, Ph.D. thesis, Georgia Institute of Technology.

Hanley, T. R., and P. G. Steffes (2007), A high-sensitivity laboratory system for measuring the microwave properties of gases under simulated conditions for planetary atmospheres, *Radio Science, 42,* doi:10.1029/2007RS003693.

Hanley, T.R., P. G. Steffes, and B. M. Karpowicz (2009), A new model of the hydrogen and helium broadened microwave opacity of ammonia based on extensive laboratory measurements, *Icarus, 202,* 316-335.

Hoffman, J.P., and P. G. Steffes (2001), Laboratory measurements of the microwave opacity of phosphine: Opacity formalism and application to the atmospheres of the outer planets, *Icarus, 152,* 172-184.

Jenkins, J. M., and P. G. Steffes (1988), Constraints on the microwave opacity of gaseous methane and water vapor in the jovian atmosphere, *Icarus, 76,* 378-382.

Karpowicz, B. M. (2010), In search of water vapor on Jupiter: Laboratory measurements of the microwave properties of water vapor and simulations of Jupiter's microwave emission in support of the Juno mission, Ph.D. thesis, Georgia Institute of Technology.

Karpowicz, B. M., and P. G. Steffes (2011), In search of water vapor on Jupiter: Laboratory measurements of the microwave properties of water vapor under simulated jovian conditions. *Icarus, 212,* 210-223.

Levenberg, K. (1944), A method for the solution of certain nonlinear problems in least squares. *Quart. Appl. Math*., Vol. 2, 164-168.

Marquardt, D. (1963), An algorithm for least-squares estimation of nonlinear parameters. *SIAM J. Appl. Math*., Vol. 11, 431-441.

Matthaei, G. L., L. Young, and E. Jones (1980), *Microwave Filters, Impedance Matching Networks and Coupling Structures*, McGraw-Hill, New York.

Pickett, H. M., R. L. Poynter, E. A. Cohen, M. L. Delitsky, J. C. Pearson, and H. S. P. Muller (1998), Submillimeter, millimeter, and microwave spectral line catalog. *J. Quant. Spectrosc. Radiat. Transfer, 60*, 883-890.

Poynter, R. L., and R. K. Kakar (1975), The microwave frequencies, line parameters, and spectral constants for NH3-14, *Astrophysical Journal Supplement Series, 29,* 87-96.

Pozar, D. M. (1998), *Microwave Engineering,* 2nd ed., Wiley and Sons, New York.

Ramo, S., J. R. Whinnery, and T. V. Duzer (1994), *Fields and Waves in Communications Electronics*, Wiley and Sons, New York.

Rodrigues, C. C., and D. Moraes Jr. (2002), Control of the emission of ammonia through adsorption in a fixed bed of activated carbon. *Adsorpt. Sci. Technol, 20,* 1013-1022.

Spilker, T. R. (1990), Laboratory measurements of microwave absorptivity and refractivity spectra of gas mixtures applicable to giant planet atmospheres, Ph.D. thesis, Stanford University.

Stillman, D. (1978), *Galileo At Work*. University of Chicago Press, Chicago.

Student, 1908. The probable error of a mean. *Biometrika, 6,* 1-25.

Townes, C. H., and A. L. Schawlow (1955), *Microwave Spectroscopy,* McGraw-Hill, New York.

Tyler, G. L., and H. T. Howard (1969), Refractivity of carbon dioxide under simulated Martian conditions, *Radio Science, 4,* 899-904.

Young, D. M., and A. D. Crowell (1962), *Physical Adsorption of Gases*. Butterworths, London.